Micro-/Nanostructured Mechanical Metamaterials

*Jae-Hwang Lee, Jonathan P. Singer, and Edwin L. Thomas**

Mechanical properties of materials have long been one of the most fundamental and studied areas of materials science for a myriad of applications. Recently, mechanical metamaterials have been shown to possess extraordinary effective properties, such as negative dynamic modulus and/or density, phononic bandgaps, superior thermoelectric properties, and high specific energy absorption. To obtain such materials on appropriate length scales to enable novel mechanical devices, it is often necessary to effectively design and fabricate micro-/nano- structured materials. In this Review, various aspects of the micro-/nano-structured materials as mechanical metamaterials, potential tools for their multidimensional fabrication, and selected methods for their structural and performance characterization are described, as well as some prospects for the future developments in this exciting and emerging field.

1. Introduction

A large part of the study of materials science is the manipulation of structure - property relationships. This pursuit, from its earliest origins has involved both manipulation of the large and small material features–architects whittled away unnecessary building material from beams while artisans melted and formed microcrystalline silica into optically transparent windows. These humble beginnings illustrate the dichotomy that is "top-down" versus "bottom-up" materials design. As time passes, the degree of control and understanding over "bottom-up" materials processing has greatly progressed. For example, ancient blacksmiths knew that specifically forged steel, such as Damascus steel,[1] could perform better in strength and sharpness, and their hidden secret was nothing more than processing to produce highly anisotropic microstructures.[2] Currently, such crystalline domains in metals are manipulated by much more advanced processing techniques enabling large defect-free centimeter single crystals to nanometer crystalline grain structures, with size optimized for materials properties such as strength and toughness.[3] These advances in processing, however, still result in a relatively stochastic material due to the interplay between kinetics of the process and the equilibrium thermodynamics of each of the many possible material structures. On the other hand, rationally designed composite structures at the macro-scale[4,5] have played a vital role in architecture, electronics, and vehicles as high-performance structural materials and their physical properties have been the subject of considerable theoretical study and optimization.[6,7]The recent strides in "top-down" deliberate structuring of materials into hierarchically organized entities attempts to extend and improve the control of structure-property relationships. More specifically, the evolution of metamaterials made from micro-/nano-structured materials (MNSM) seeks to develop entirely new, or greatly enhanced material behaviors by rational design.

The concept of metamaterials was first introduced in the field of electromagnetic (EM) materials.[8–10] Here it came to mean a material whose effective properties arose not from the bulk behavior of the materials which composed it, but more from their deliberate structuring. Therefore, metamaterials sit at the intersection of two classical categories, materials and devices. Our definition of metamaterials in this review is somewhat broader than what conventionally defined as it includes all MNSMs regardless of a relative scale ratio between the characteristic structural length and the wavelengths of EM or mechanical waves. In the conventional (narrower) definition of metamaterials, the characteristic length scale of their structures is one or more orders smaller than the wavelengths. Therefore the metamaterials structure can be considered as a homogeneous effective medium. An illustrative example is the contrast between a silicon ingot, a photonic crystal, and a microprocessor (**Figure 1**). In the case of the single crystal Si ingot, the materials properties are determined completely by the behavior of the silicon atoms and their space group. The silicon microprocessor is a device whose functionalities arise from the combination of extremely organized circuitry, applied fields and multi-material devices along with precise addition of dopant atoms. The photonic crystal is still chemically pure silicon, however, its woodpile-like artificial geometry leads to dramatic alteration of the EM-wave propagation through the structure. In this way the work of the artisan has met that of the architect in creating a material whose deliberate structuring leads to effective properties

Prof. E. L. Thomas, Dr. J.-H. Lee
Department of Mechanical Engineering
and Materials Science
Rice University
6100 Main St. Houston, Texas 77005 USA
E-mail: elt@rice.edu
J. P. Singer
Department of Materials Science and Engineering
Institute for Soldier Nanotechnologies
Massachusetts Institute of Technology
Cambridge, MA 02139 USA

DOI: 10.1002/adma.201201644

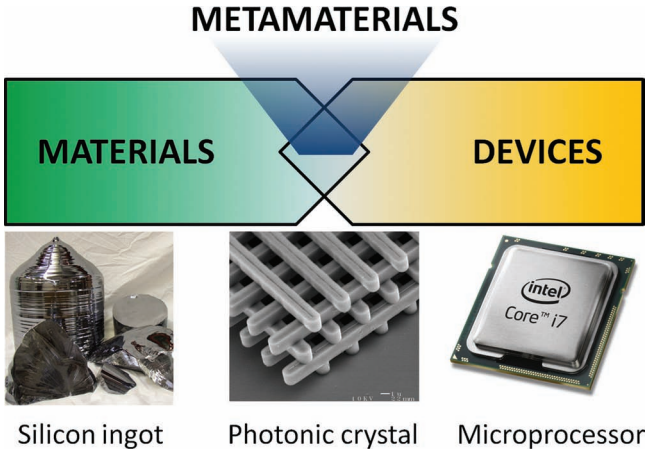

Figure 1. Concept of metamaterials. Images courtesy of ref. [12].

of unprecedented nature; more precisely, EM waves of a specific band of frequencies are 100% reflected from the otherwise transparent silicon structure. These optical metamaterials have been utilized to manipulate light in counterintuitive, fantastical ways: slowing the speed of light, reversing its refraction, and creating arbitrary paths to distort or cloak an object.[11]

The metamaterial concept has recently been extended to many other material properties, including materials to achieve novel *mechanical* behaviors. Various applications include for example, phononic crystals, acoustic metamaterials, and auxetic materials. **Figure 2** shows two different structures made of carbon: one is a carbon foam and the other is a carbon MNSM. From the material-centric standpoint, both are low density cellular or porous materials. Traditionally, cellular materials have been used in a variety of light-weight structural material applications. Generally conventional cellular materials are produced by stochastic processes and thus, their structural parameters including cell topology, cell size, and a ligament size are given by a statistical average.[13,14] Since the last decade, the advance of designer MNSM has allowed for the reduction of cell size down to the nano-scale and for the ordered arrangement of the cell positions and choice of the structural symmetry. As demonstrated in Figure 2b, MNSMs distinguish themselves by more precise and rational designed geometries and compositions, often with a significantly smaller feature size, which will eventually enable unprecedented material behaviors deviating from the extrapolated expectation of conventional knowledge.

Compared to conventional irregular foams, the mechanical properties of the MNSMs are more predictable by use of numerical simulations due to their well ordered geometries. However, in actuality, the scalability is limited by the actual mechanical responses of the MNSM because the response depends not only on the geometrical structure, but also on the complex interactions of the geometrical structure with constituent materials, their interfaces and, in the case of mechanical deformations, the length scales of the attendant plastic processes relative to the length scales in the structured material. At the macro-scale, the only factor limiting the scalability is gravity (i.e. the ability for the structure to support itself). As the feature size of a structure becomes smaller, other factors become relevant: (1) Internal structures - At large length scale, the internal structure of the constituent materials such as crystal domains and defects are averaged into a hypothetical effective material. As the scale of a geometrical structure approaches that of the internal structures of the constituent

Jonathan P. Singer received his B.S. and M. S. degrees in Materials Science and Engineering from the University of Pennsylvania in 2008. He is currently pursuing his doctorate in the group of Prof. E. L. Thomas at the Massachusetts Institute of Technology. His research is on the development of hybrid large area and direct write lithographic techniques for the rapid fabrication of 3D micro/nano structured materials.

Dr. Jae-Hwang Lee is currently a research scientist in the Department of Mechanical Engineering and Materials Science at Rice University since 2011. He received his Ph.D. in Condensed Matter Physics at Iowa State University in 2006. He moved to the Massachusetts Institute of Technology in 2007 as a postdoctoral researcher. His research interests focus on 3D nano-fabrication techniques, mechanical characteristics of periodic nanostructures, thermophotovoltaics using photonic crystals, and guided self-assembly.

Dr. Edwin L. Thomas is currently Dean of Engineering at Rice University in Houston and a professor in Mechanical Engineering and Materials Science. He received his Ph.D. in Materials Science and Engineering at Cornell in 1974. Thomas was department head of Materials Science and Engineering at Massachusetts Institute of Technology from 2006–2011. His research is in polymer physics and self-assembly, engineering photonic crystals, phononic crystals, metamaterials, microtrusses and 3D structure formation via direct write and interference lithography techniques.

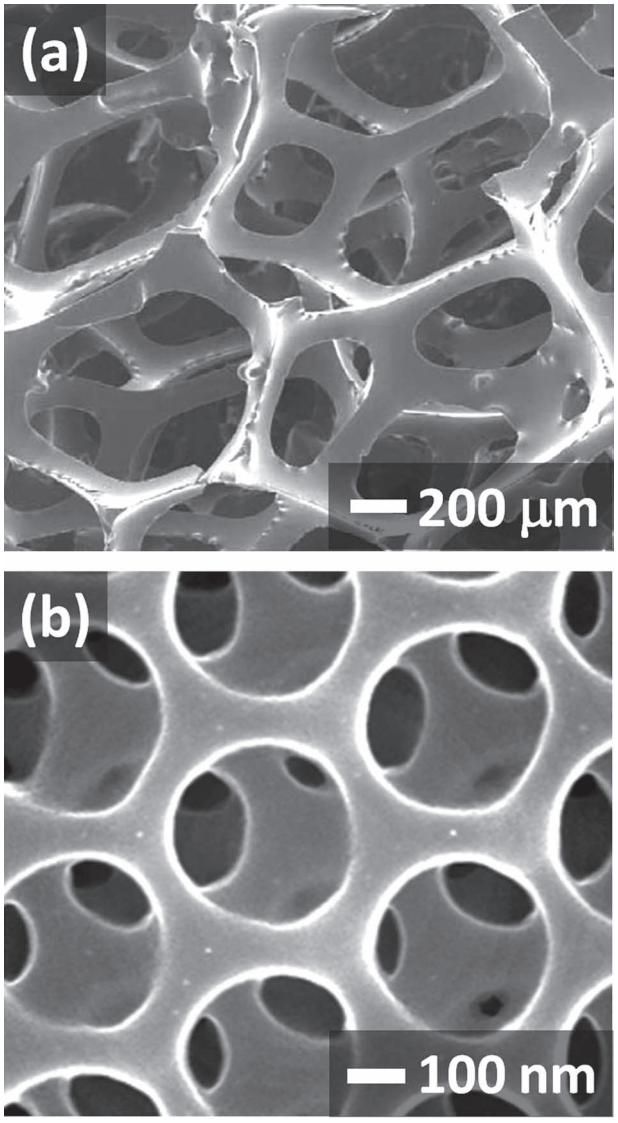

Figure 2. SEM images of cellular carbon structures. (a) A vitreous carbon foam of randomly distributed open cells for thermal management. Reproduced with permission.[15] Copyright 2002 Pergamon. (b) A carbon MNSM created by carbonization of a polymer template in our lab for energy absorption. Note that the MNSM possesses a face-centered-cubic-like structure and a 1500× smaller feature size than the carbon foam.

materials, effective material properties cannot be applied and the actual mechanical characteristics strongly depend on the local interactions between the geometrical structures and the internal structures. (2) Specific surface area - the surface area per unit volume of a periodic structure increases as its periodicity decreases, while the surface area per unit cell remains same. Consequently, surface phenomena which are negligible at the macro-scale may play an important role. (3) Stimuli–due to the wave-like nature of some stimuli such as elastic and EM waves, the material properties arising from the interaction with such stimuli cannot be scalable as both the stimulus and the material structure posses a characteristic size.

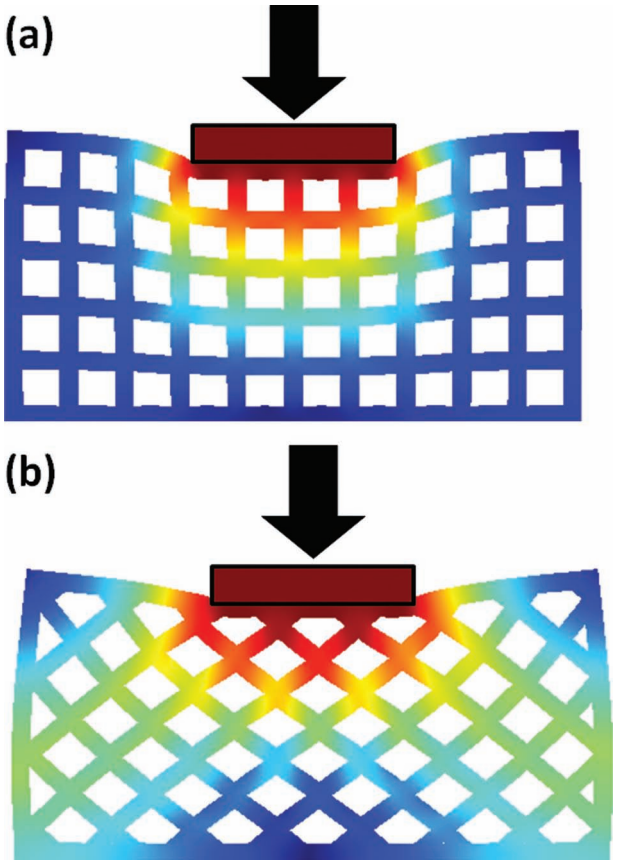

Figure 3. True strain distributions in a 2D frame from the same external displacement depending on loading in the (a) [10] and (b) [11] directions.

Another important aspect of MNSM is the ability to design for structural anisotropy. Many natural structural materials are highly mechanically anisotropic, for instance, the shell of an abalone,[16] the exoskeleton of a lobster,[17] and human bones.[18,19] As a result, bone, for example, can exhibit nearly 20 times higher elastic modulus and tensile strength along the axial direction compared to the transverse direction. Thus, structural anisotropy as in the ancient Damascus steel blades can be an essential factor in the improvement of mechanical performance without a change in chemical composition or weight. Modern structures of MNSMs can now of course be much more exactly controlled. **Figure 3** shows simulated strain distributions of a 2D square lattice depending on the direction of loading. Due to structural anisotropy, for the same external displacements, a much broader local strain distribution is observed for loading along the [11] direction than along the [10]. Moreover, as seen in Figure 3b, a designed structural anisotropy can guide the loading into certain directions/features. Thus, one can expect MNSMs could be designed to create complex stress-strain paths to protect a certain internal volume by using more sophisticated control of the structural anisotropy.

Compared to interactions between light and matter in EM-metamaterials, which are mostly linear and well described by vectorial equations, mechanical interactions in MNSMs are frequently associated with parameters that generally require

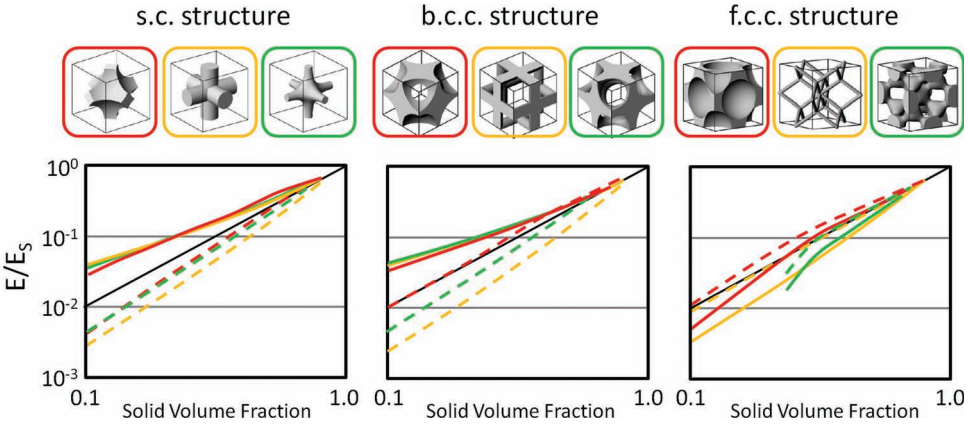

Figure 4. Young's modulus for families of cubic symmetry structures based on air-spheres (red line), connected-rod models (yellow line), and level set structures (green line) as a function of solid volume fraction. The results are normalized with respect to the Young's modulus E_S of the solid material that forms the periodic structure. Solid lines and dashed lines correspond to the Young's modulus along the <100> and <111> directions, respectively. Solid black lines given by Equation (1) for open-cell foams. Reproduced with permission.[22]

tensorial equations. The complexity arising from the coupled interactions is a great challenge in design, fabrication, and analysis; however it allows one to develop unprecedented multifunctional mechanical materials. In this review, we intend to provide some background, insights and future directions into various mechanical aspects of the MNSMs with their potential fabrication methods and structural and performance characterization techniques.

2. Characteristics of the MNSMs

This section reviews several relevant mechanical characteristics of MNSMs and makes the distinction between linear and nonlinear effects.

2.1. Static Modulus and Density

We now discuss the static modulus and density of MNSMs, corresponding to strain rates where the materials properties do not deviate significantly from their asymptotic limit as the strain rate goes to zero. The dynamic modulus and density will be discussed in the acoustic/phononic section. The static modulus of conventional cellular materials as a function of density has been extensively studied.[13–14,20–21] The relative Young's modulus (E/E_S) as a function of relative density is given by[20]

$$E/E_S \sim (\rho/\rho_S)^2 \quad \text{(open cell)} \tag{1}$$

$$E/E_S \sim (\rho/\rho_S)^3 \quad \text{(closed cell)} \tag{2}$$

where, E_S and $\rho_S$are the Young's modulus and the density of the solid material.

These approximate equations have no dependence on either the length-scale or the specific symmetry of the structure. For MNSM both these additional considerations are critically important for determination of the overall anisotropic materials properties. Maldovan *et al.* calculated density-dependent modulus for several representative cases including the three cubic structures: simple cubic (s.c., $Pm\bar{3}m$ space group), body-centered-cubic (b.c.c., $Im\bar{3}m$ space group), and face-centered cubic (f.c.c, $Fm\bar{3}m$ space group), as shown in **Figure 4**.[22] Three types of models were studied: air-spheres, rod-connected models and level set structures[23] The s.c. and b.c.c. structures are made of 6 and 4-connected nodes respectively, while the f.c.c. case has two types of nodes–4-connected tetrahedral and 8-connected octahedral nodes. The normalized Young's modulus, shows structural anisotropy between the <100> and <111> directions, especially for the s.c. and b.c.c. structures. Even within the same class of lattices, the difference among the three kinds of structures is largest for the <111> direction. Indeed, the general scaling behavior of modulus to density for open-cell materials is not adequate for the MNSMs. Moreover, consistent with these theoretical predictions, experimentally fabricated epoxy MNSMs by Lee *et al.* with f.c.c symmetry showed a scaling exponent of 1.26 rather than the predicted 2.0 for the <111> direction in spite of its open and cubic symmetry cell geometry.[24] A smaller scaling exponent indicates less loss in elastic modulus for decreased relative density. Structural anisotropy is responsible for this discrepancy and this aspect should be emphasized in the design of non-conventional cellular materials by use of MNSMs. The anisotropy degree can also be well tailored and tuned by the beam/strut diameter ratio in MNSMs at a given density.[25]

Extremely low density materials are an interesting class of materials as they can have very limited heat conduction paths due to their thin ligaments and necks as well as high specific surface area. However, a common challenge of such low density materials like aerogels is that their scaling exponent ranges from 3 to 4, larger than for closed-cell structures in Equation (2). Consequently these structures are very fragile and can bear only very small loads compared to conventional foams. Numerical simulations suggest that the high scaling exponent is largely due to the reduction in the connectivity of the material with decreasing density and not due to dangling (unconnected) mass which causes increase of density

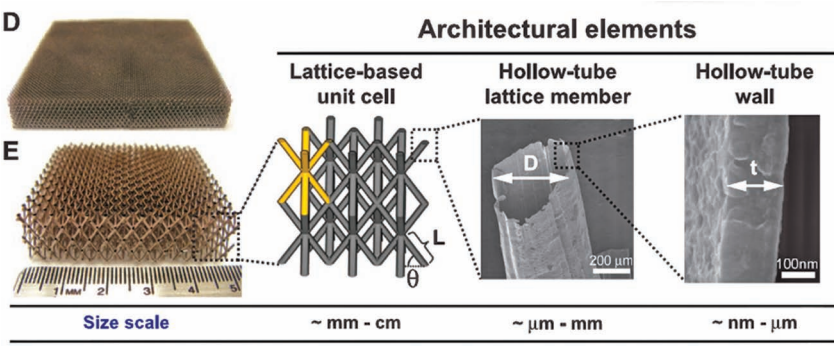

Figure 5. Images of two as-fabricated hollow tubular frames along with illustration of the relevant architectural elements. Reproduced with permission.[27] Copyright 2011 Science.

without contribution to structural deformation.[26] Therefore, the open-cell model, which predicts a scaling exponent of 2, may be valid only when the connectivity remains unchanged upon variation of the density. Recently Schaedler *et al.* demonstrated a frame comprised of hollow struts (see **Figure 5**) that follows the scaling law in Equation (2) even though its density is as low as 9×10^{-4} g/cm^3.[27] The improvement in mechanical strength over the previous low density materials, is achieved by well-controlled dimensions and periodicity of the architecture. From such macroscopic (mm scale) demonstrations, we can expect similar approaches would be possible using MNSMs to achieve extremely low density with good mechanical strength simultaneously.

2.2. Specific Energy Absorption

Cellular materials made of polymers, metals and ceramics have been used as structural materials due to their superior mechanical strength, stiffness and energy absorption over corresponding solid materials,[13,28,29] and have also been proposed for multifunctional materials for an air-breathing hypersonic vehicle to provide both a light-weight and structurally strong frame with an efficient heat exchanger.[30] In this section, we discuss the possibility of MNSMs for enhancing the energy absorption per unit weight, or specific energy absorption (SEA). Compared to conventional cellular materials, MNSM can be fabricated to possess a geometry, feature size, and asymmetry to maximize plastic deformation and fractures, an essential aspect when very stringent limitations in overall material thickness (areal density) is required. Wang *et al.* numerically assessed plastic deformation of the MNSM with various modeled structural parameters and showed how the optimization of the studied parameters can maximize energy absorption.[25] Subsequently Lee *et al.* experimentally demonstrated how manipulation of the structural design can help to create better energy absorbing materials.[24] In this study, it was shown that an epoxy MNSM has a more concentrated stress distribution when its volume fraction is low, and that this distribution leads to shear deformation at the struts of the MNSM where the stress concentration is highest (**Figure 6**). Thus, a 25% increase in SEA is experimentally achieved by reducing the density by 20%.

Interpenetrating phase composites (IPCs)[31] are topologically equivalent to an open-cell structure whose air space is substituted with a second material, leading to physically interlocked phases as demonstrated at the macro-scale.[32] Although most examples to date of MNSMs have a single solid phase, two or more phase MNSMs are also possible to create, resulting in periodic bi- or multi-composites. Various combinations of different materials can be imagined such as polymer-ceramic and metal-ceramic systems. Inspired by nanomechanical heterogeneity that is used to enhance energy dissipation in natural structures,[33] the combination of hard and soft materials is expected to improve the SEA significantly. For example, a brittle carbon MNSM fabricated by carbonization[34,35] of an photoresist becomes a bicontinuous MNSM composite if its air phase is appropriately infiltrated by chemical vapor deposition[36] or by infusion of a molten material such as polymer[37] or aluminum. In a MNSM solid/solid bi-composite, stress transfer and strain matching between the different phases are expected and this can lead to an increase in the observed failure strain by both limiting crack propagation and redistributing the local stress. Furthermore, when the MNSM does fail, more mechanical energy can be dissipated by enabling a multitude of cracking events. These highly engineered MNSM composites may be useful for shielding layers in soldier protection, space applications and hypersonic aircraft where stringent limitations in material thickness and weight are present.

It is well known that the grain size plays an important role in metals; the most notable example being the Hall-Petch relationship which describes the increase of mechanical yield strength (or hardness) with decreasing mean grain size.[38,39] This reflects how the increased density of grain boundaries impede dislocation activity until the emergence of glass-like shear banding at grain sizes below 20 nm.[40] The effects from the material's internal structure should thus be considered for the prediction of the behavior of MNSMs. Depending on fabrication and processing conditions, the large internal surfaces of the MNSMs can act as artificially introduced grain boundaries; thus higher SEA capability is expected by reducing the periodicity and feature size of MNSMs.

2.3. Acoustic/Phononic Metamaterials

The engineering of the propagation behavior of mechanical waves, including acoustic waves, has been extensively studied in the fields of sound and vibration control and is currently employed in a broad range of applications; for example, sophisticated sound engineering structures found in auditoriums, medical imaging devices using ultrasonic waves, and submarine hull design. As most materials used for the engineering of sound dissipate and reflect the incident waves over a broad range of frequencies, they are optically analogous to black and white surfaces respectively. Next we discuss how materials can be engineered to give a specific chromatic response to mechanical waves without dissipating their energy.

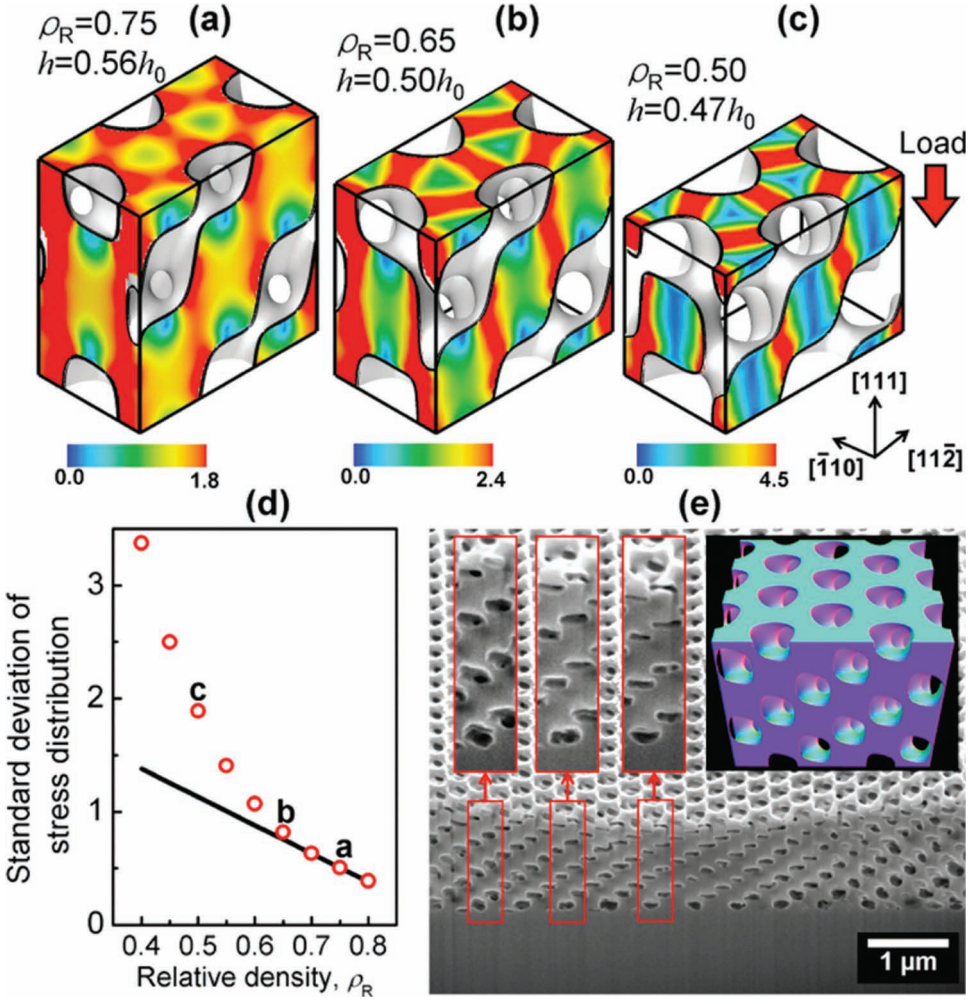

Figure 6. Theoretical von Mises stress distributions of MNSMs for three different values of the volume fraction (a) 0.75, (b) 0.65, and (c) 0.50, respectively. All samples are loaded with the same compressive stress along the [111] direction. The level of stress is normalized to that of the 100% solid. (d) The standard deviation of the local stresses within a single unit cell as a function of the volume fraction represents the degree of concentration of the stress (red circles). The three deviations corresponding to the stress maps in (a–c) are marked with the same figure letters. (e) A cross-sectional SEM image (52° tilt) of a focused ion beam milled MNSM after plastic compressive loading shown along with magnified images of three selected regions at increasing sample plasticity. Reproduced with permission.[24] Copyright 2010 American Chemical Society.

Mechanical waves create a temporal change of the local density of a material and include (the scalar) acoustic wave in fluids and (the 3D vector) elastic wave in solids. In contrast to the two polarizations of an EM wave, the mechanical wave cannot propagate in vacuum and has three polarizations within a solid. In a homogeneous, isotropic solid medium, the propagating waves consist of one longitudinal mode and two transverse modes and the speeds of sound for transverse and longitudinal elastic plane waves, c_T and c_L are given by the relations:

$$c_T = \sqrt{\frac{\mu}{\rho}},\ c_L = \sqrt{\frac{\lambda + 2\mu}{\rho}} \tag{3}$$

where ρ is the density, and λ and μ are the Lamé coefficients, which are related to Young's modulus (E) and Poisson's ratio (ν) of the solid by the following equations:

$$\lambda = \frac{E\nu}{(1+\nu)(1-2\nu)},\ \mu = \frac{E}{2(1+\nu)} \tag{4}$$

Note that the transverse and longitudinal plane waves are independent of each other and the longitudinal wave is always faster.

A wave propagating through the set of interfaces between two different materials in a bi-composite is reflected or transmitted at the interfaces between two materials having different mechanical impedance given by:

$$Z = \rho c = \sqrt{\rho(\lambda + 2\mu)} \tag{5}$$

where c is a speed of sound (either c_T or c_L). Reflectance (R) and transmittance (T) for a normal incidence wave at the interface of two lossless materials having impedances of Z_1 and Z_2 are determined by the equations:

$$R = \frac{4Z_1Z_2}{(Z_1+Z_2)^2} = \frac{4Z_1/Z_2}{(Z_1/Z_2+1)^2} \quad (6)$$

$$T = \frac{(Z_1-Z_2)^2}{(Z_1+Z_2)^2} = \frac{(Z_1/Z_2-1)^2}{(Z_1/Z_2+1)^2} \quad (7)$$

where $R + T = 1$, implying energy conservation. The reflectance and transmittance are independent of the frequency of the mechanical wave for homogeneous materials. Moreover, by choosing a fluid and a solid as the two media, the impedance ratio Z_1/Z_2 can be either very small or very large, thus reflectance approaches zero or unity depending on which material the wave is propagating from.

Mechanical waves propagating through an inhomogeneous medium experience spatially varying mechanical properties and thus undergo multiple reflection events. If the variation of mechanical properties is periodic, systematic interference between the transmitted and the reflected waves occurs and, as a result, changes the propagation behavior of the mechanical wave depend on its frequency relative to the structural periodicities. Because all mechanical waves can be represented by eigenmodes of vibration (phonons) and periodic impedance media can alter the density of states for the phonons, such periodic structures are often called *phononic crystals*. The dispersion relation, $\omega = \omega(\mathbf{k})$ for the phononic crystal can be obtained by numerically solving the elastic wave equation,

$$\rho\frac{\partial^2 u_i}{\partial t^2} = \nabla\cdot\left(\rho c_T^2\nabla u_i\right) + \nabla\cdot\left(\rho c_T^2\frac{\partial \mathbf{u}}{\partial x}\right)_i + \frac{\partial}{\partial x_i}\left[\left(\rho c_L^2 - 2\rho c_T^2\right)\nabla\cdot\mathbf{u}\right] \quad (8)$$

The vector displacement field ($\mathbf{u}$) is given by the Bloch wave,

$$\mathbf{u_k}(\mathbf{r}, t) = \mathrm{Re}[\mathbf{f_k}(\mathbf{r})e^{i(\mathbf{k}\cdot\mathbf{r}-\omega(\mathbf{k})t)}] \quad (9)$$

where $\mathbf{r}$ and $\mathbf{k}$ are position and wave vectors and $\mathbf{fk}(\mathbf{r})$ is a vector function correlating with the periodically varying impedance, which is invariant under any translation given by a lattice vector $\mathbf{R}$:

$$\mathbf{f_k}(\mathbf{r}) = \mathbf{f_k}(\mathbf{r}+\mathbf{R}) \quad (10)$$

In contrast to wave propagation through a homogeneous medium, a propagating wave within a phononic crystal is generally neither purely transverse nor purely longitudinal. A more detailed description can be found elsewhere.[41]

The degree of modification of the phonon dispersion by the spatially varying mechanical properties (impedance) is proportional to the Z contrast. Since this can be quite high (especially between solid and air), significant effects are expected with a small repeat-number of unit cells of phononic crystals, unlike the case of photonic crystals where the refractive index contrast is much lower and the number of unit cells necessary for significant influence is correspondingly larger. Of interest to the design of MNSM, hypersonic mechanical waves are those with wavelengths less than 10 μm, which correspond to frequencies higher than 100 MHz. The hypersonic phonons are relevant to important physical phenomena such as spontaneous photon emission in intrinsic silicon. Greater control over the phonons in silicon could lead to more efficient light emitting devices.[42] Moreover, as the hypersonic phonons are related to random thermal motion of atoms, phonon contribution in heat conduction could be altered.[43] A phononic bandgap, a range of energies (or frequencies) for which there are no propagating phonons is shown in **Figure 7**.[44] The transmission of mechanical waves through the phononic crystal slab shows a strong frequency dependence and transmission is significantly lower over a certain range of frequencies (120 ~ 150 MHz) due to the phononic bandgap or, more generally, the frequency dependent impedance of the phononic crystal.

The phonon dispersion relation, $\omega(\mathbf{k})$ can be measured by angle-dependent inelastic light scattering. **Figure 8** shows the experimentally measured dispersion of a 2D phononic crystal comprised of a square lattice of air hole cylinders in an epoxy matrix on a glass substrate using Brillouin light scattering (BLS),[45] which will be discussed later in detail. In this study, the dispersion curve of phonons was strongly bent near the first Brillouin zone and a phononic bandgap is opened around 1.4 GHz (Figure 8c). In 3D phononic crystals made of

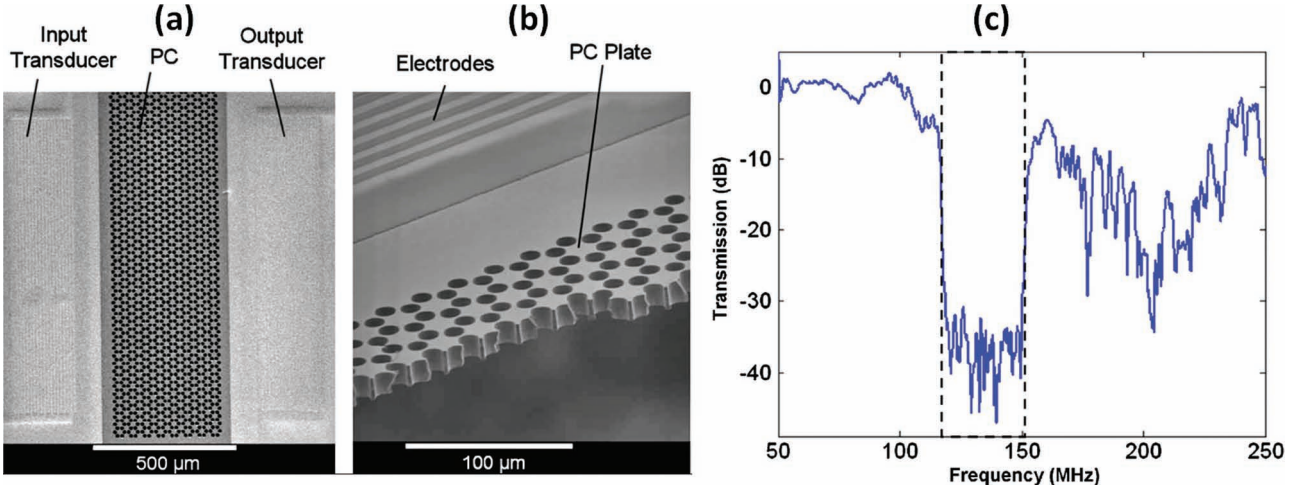

Figure 7. (a) A 2D phononic crystal made of a hexagonally perforated silicon slab (a) top view (b) cross sectional view (c) Transmission spectrum of the phononic crystal displaying a bandgap centered at ~130 MHz. Reproduced with permission.[44] Copyright 2008 American Institute of Physics.

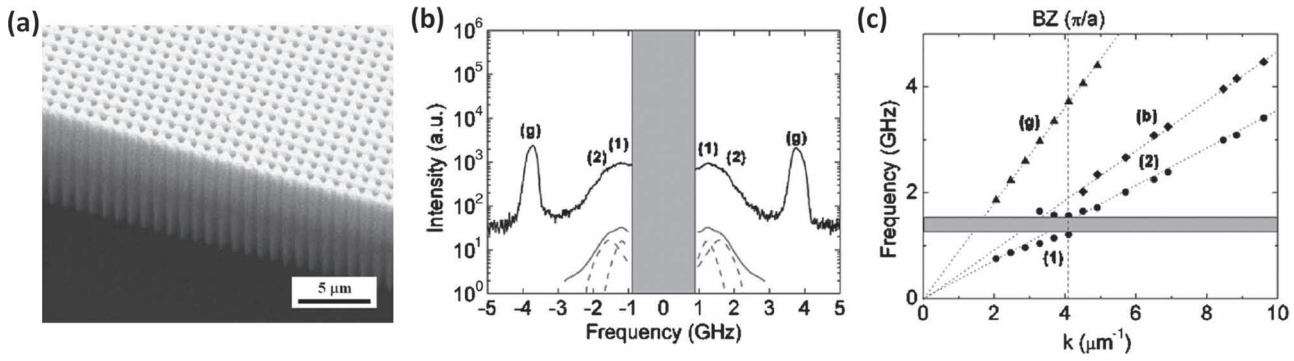

Figure 8. (a) SEM image of a cross section of the 2D square air cylinder crystal. The lattice constant was 750 nm and the radius of the holes was 250 nm resulting in 35% air volume fraction. (b) BLS spectrum taken at $k = 4.1\ \mu m^{-1}$ that corresponds to the edge of the first Brillouin zone along the [10] direction. It can be seen that in this case two modes are present: (1) and (2). (d) Phononic dispersion relation along the [10] direction showing a partial bandgap between 1.21 and 1.57 GHz (in gray). Reproduced with permission.[45] Copyright 2007 American Institute of Physics.

self-assembled silica microspheres, partial phononic bandgaps have been demonstrated at ~5 GHz.[43] Further, unusually flat phononic band behavior due to coherent multiple scattering effect interactions rather than localized single-particle resonance was found in these systems.[46]

Interesting physical phenomena also occur at sonic and ultrasonic frequencies. Elastic constants of materials should be positive in static stress, however *negative* elastic constants for time-varying stresses have been demonstrated. This phenomena can be qualitatively understood by the out-of-phase relation between time-varying stress and corresponding strain and resultant reflection of propagating waves even though the materials are effectively considered as a homogeneous medium due to the several order of magnitude difference between the wavelength of the propagating wave and the scale of the local structure.[47] For example, materials consisting of individual resonators made of high-density metal cores implanted in uniform elastically soft matrixes first demonstrated a negative elastic constant at frequencies, $f < 1,000$ Hz for elastic waves in solid.[48] An array of Helmholtz resonators with designed acoustic inductance and capacitance also showed dynamic negative modulus at higher frequencies (near 30 kHz), in a fluid.[49] Theoretical works showed that such mechanical metamaterials can simultaneously exhibit both negative density and negative bulk modulus and therefore negative refractive indices for acoustic waves are possible.[50–53] It is important to note, however, that the detailed structural designs necessary for these negative index materials are quite exotic, often featuring floating gas or liquid domains within the solid structure. Negative index may also be obtained by manipulating the band structure as in the phononic crystals discussed above. In this way, focusing ultrasound waves using a flat mechanical metamaterial lens has experimentally demonstrated negative refractive index effects.[54] Furthermore, organized acoustic inductor and capacitor structures were utilized to demonstrate an acoustic cloak for underwater ultrasound waves[55] (**Figure 9**). Interestingly, compared to the rather narrow range of cloaking frequencies reported for EM cloaks,[56] the acoustic cloak demonstrated a broad range of frequencies over $\Delta f/f_C \sim 20\%$ at 52 to 64 kHz, where Δf and f_C are the range of cloaking frequencies and the center frequency of the range. More recently, Stenger *et al.* also achieved broad working frequencies of over 100% at audible frequencies (200 ~ 400 Hz) using a structure made of 2D composite of hard and soft polymers.[57] In this study, much as with the negative lensing discussed above, the broad range acoustic cloaking was possible by structures consisting of non-resonant elements through dispersion manipulation.

2.4. Heat Transport

Heat conduction by phonons is the dominant mode of thermal transport in non-metallic solids; however for MNSM, thermal transport can be strongly modified and/or radiative transfer may be induced. Engineering thermal conductivity by MNSMs is one strategy for improving the power generation of thermoelectric devices. The thermoelectric figure-of-merit (Z) is related to the Seebeck coefficient (S), electrical conductivity (σ), and thermal conductivity (k) by the equation,

$$Z = \frac{S^2\sigma}{k} \tag{11}$$

To achieve a large Z value for high efficiency thermoelectric devices, a low thermal conductivity, but high electrical conductivity and large Seebeck coefficient are desirable. Since high electrical conductivity is required to minimize Joule loss, reducing thermal conductivity is key. Multilayer superlattices, technically 1D MNSMs, have been proposed to reduce thermal conductivity by enhancing phonon scattering.[58] A number of other approaches to scatter phonons have also been investigated and recently reviewed.[59–61] Since the wavelengths of dominant phonons are on the order of nanometers, as seen in **Figure 10**, MNSMs using self-supporting 3D morphologies of block copolymers (BCP)[62,63] can be a practical choice. The phase-separated BCP can be processed by crosslinking, etching, and substitution to remove one phase and to convert the other phase, while preserving the nano-scale 3D periodic morphology. Similar techniques have been adopted for design of optical materials.[64,65]

In conventional far-field radiative heat transfer, the radiative heat flux between two infinite plates at different temperatures

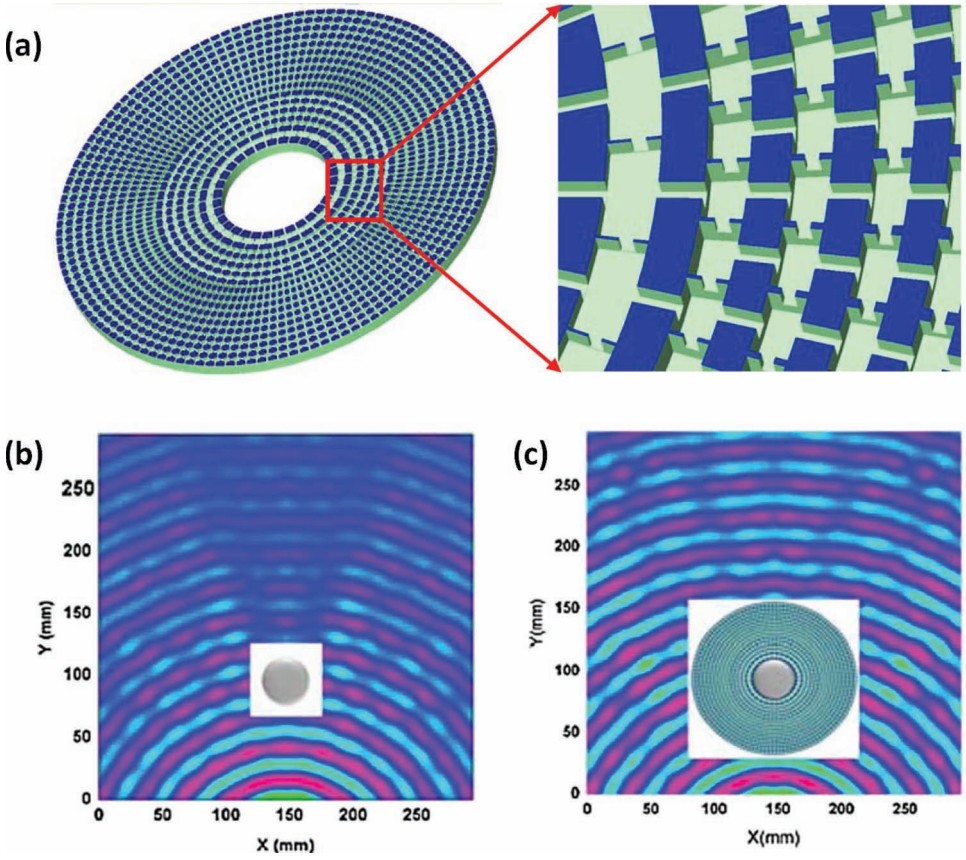

Figure 9. Acoustic cloaking. (a) The configuration of the acoustic cylindrical cloak. Measured pressure field mappings of (b) the bare steel cylinder (note shadow region behind cylinder) and (c) the cloaked steel cylinder illuminated with a point ultrasound source at 60 kHz. Reproduced with permission.[55] Copyright 2011 American Physical Society.

separated by a vacuum gap is given by the Stefan-Boltzmann law, $\xi(T^4_1 - T_2{}^4)$ where T_1, T_2, are high and low temperatures of the two plates, and ξ is the Stefan-Boltzmann constant. The law is valid when a distance between the two plates is much greater than the dominant wavelength of thermal radiation given by Wien's displacement law (see Figure 10a), which is the usual situation. However, if the distance between plates is smaller than the dominant wavelength, the heat flux through near-field transfer surpasses that of the far-field as demonstrated by both numerical calculations and experiments.[66–68] The plot in Figure 10b in fact shows that the near-field heat transfer is very efficient for all sub-micron gaps. Thus, if we create a MNSM having a very limited thermal conduction, for example by using very thin connections between structural elements, its effective thermal conductivity is the combination of heat conduction and temperature-dependent near-field radiation. This allows for the tuning of the overall temperature-dependent characteristics of heat transfer and can be applied to create a thermal rectifier.[69]

Metallic MNSMs (e.g. metallic photonic crystals) can also control far-field thermal radiation characteristics by engineering the intrinsic absorption of metals.[70] Generally metals are a poor thermal emitter; however, their emissivity can be dramatically enhanced at a specific range of wavelengths by introducing MNSMs which work like artificial atoms resonating at the specified wavelengths.[71,72] A tungsten MNSM with a woodpile-like geometry (**Figure 11**) emits thermal radiation at selected wavelengths when it is Joule-heated by passing current compared to the broad spectrum emitted from a flat homogeneous tungsten film. Besides spectral engineering, angular distribution[73] and polarization[74–76] of the thermal radiation can also be designed. Compared to the original fabrication approach using typical semiconductor processes, which are typically a layer-by-layer approach and thus, time consuming and expensive, several alternative approaches using soft lithography[77] and direct laser writing are promising.[78] These techniques will be discussed in detail below.

One of the important applications of MNSMs is a spectrum converter for thermophotovoltaic devices. While the typical blackbody radiation spectrum is very broad, photovoltaic devices that utilize semiconductors rely on a very narrow absorption spectrum given by the electron energy bandgap. Thus, a photon carrying energy less than the bandgap does not create an electron-hole pair and its energy dissipates without contribution to power generation. For energies greater than the bandgap, every photon creates a single electron-hole pair regardless of its energy, consequently the excess amount of energy exceeding the bandgap is also wasted by non-radiative processes. The energy loss from the spectral mismatch is the most significant

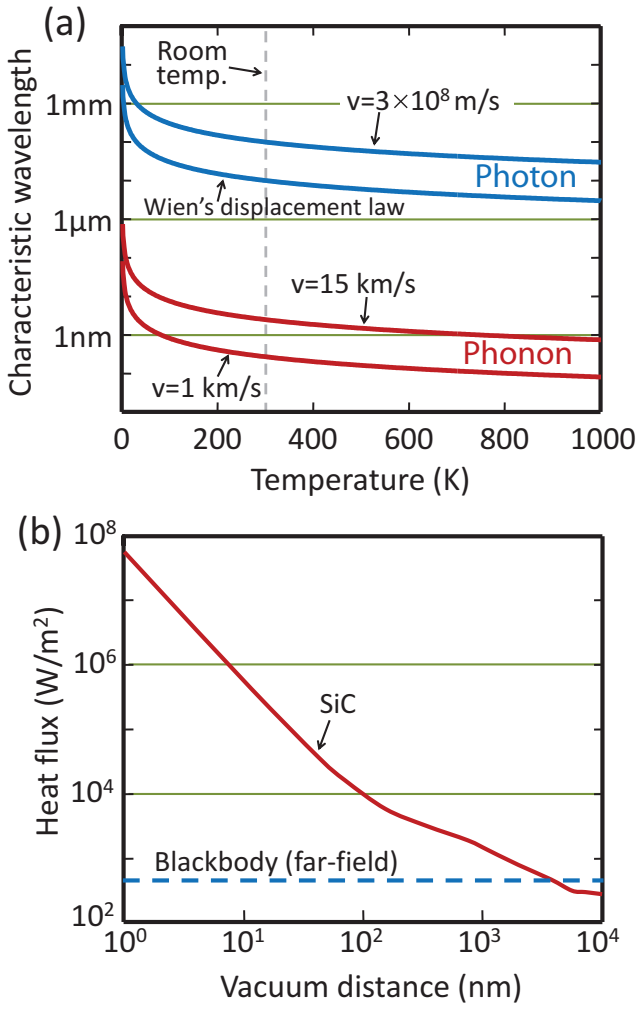

Figure 10. (a) Dominant characteristic wavelengths for phonons, photons, and electrons depending on temperature. The phonon wavelength is estimated by $k_B T/2 \sim h\nu/\lambda$ for two possible high and low speeds of sound (ν) in solid, where k_B is the Boltzmann constant and h is the Plank constant. Similar estimation curves for photons are plotted with $k_B T/2 \sim hc/\lambda$ and Wien's displacement law, where c is the speed of light in vacuum. (b) Radiative heat transfer as a function of gap distance between two infinite SiC plates maintained at 300 and 0 K. The far-field energy transfer between two blackbodies has also been shown for reference. Reproduced with permission.[66]

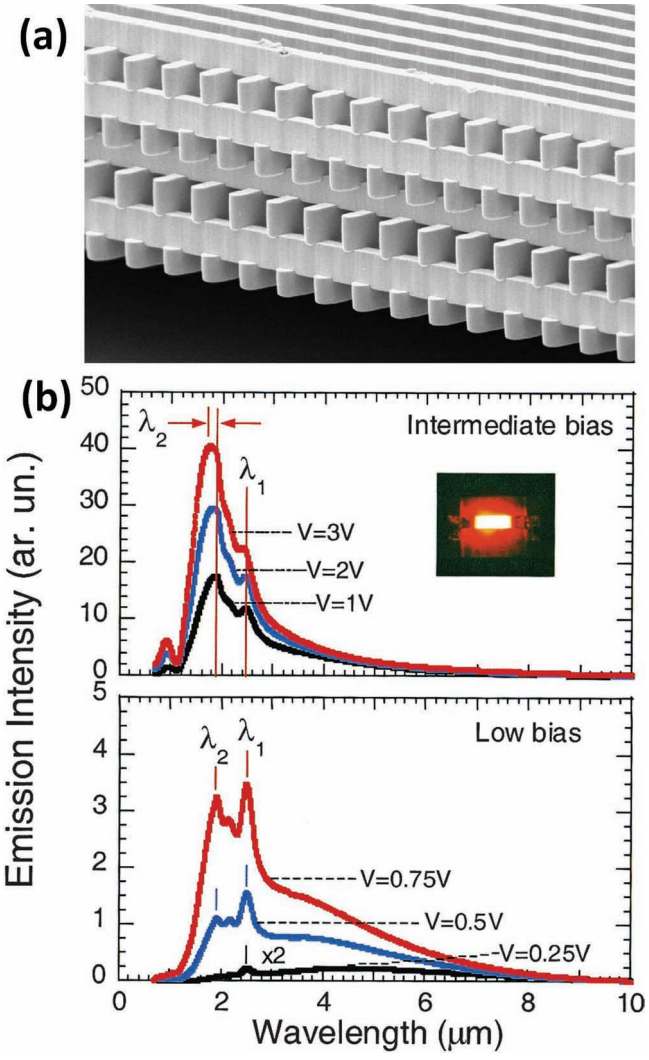

Figure 11. (a) SEM image of a 3D tungsten photonic crystal. Within each layer, the one-dimensional rod width is 0.5 um and the rod-to-rod spacing is 1.5 um. (b) Thermal emission spectra taken at low and intermediate bias. Reproduced with permission.[71] Copyright 2003 Optical Society of America.

reason limiting the efficiency of photovoltaic devices when a broad radiation spectrum is used such as sunlight or IR radiation from a waste heat source. Suppose a box made of metallic MNSMs and that this MNSM box has a small opening at one face. The sunlight can then be focused to the entrance and most radiation energy will be eventually absorbed within the box and elevate the temperature of the box. Because the surface of the MNSM box will emit thermal radiation at the elevated temperature through the selective wavelengths, the conversion of the broad spectrum to a narrow one can be accomplished. In addition, using metallic MNSMs, one can design a smart surface that can dissipate heat through tunable ranges of wavelengths and tunable angles with a specific polarization. This capability is also potentially important in military and security applications. There are however certain technical difficulties including structural stability of the materials at high temperature. Such difficulties are expected to be solved by choosing proper materials. For instance, Nagpal *et al.* attempted an approach using a two-materials system: metal-coated carbon MNSMs to achieve both high temperature stability and an advantageous optical property.[79]

2.5. Negative Poisson's Ratio

Poisson's ratio (ν) is the ratio of transverse strain to the axial strain. Counter-intuitively, materials having *negative* ν or auxetics[80] expand in the unstressed direction under uniaxial stretching. Auxetic materials are known to exhibit enhanced mechanical characteristics not expected from their conventional

counterparts. A well-known example is the shear modulus (G), which for a homogeneous isotropic material is given by a function of Young's modulus and ν:

$$G = \frac{E}{2(1+\nu)} \tag{12}$$

For an auxetic material with ν approaching -1, the shear modulus diverges making indentation exceedingly difficult. This unique behavior of an auxetic material flowing *into* the vicinity of the impact rather than flowing away in the lateral direction[81] can be applied to improve protective materials or energy absorbing materials.[82] Furthermore, such auxetic materials can also be applied as a efficient membrane filter with variable permeability,[83,84] fasteners,[85,86] shape memory materials,[87] and acoustic dampeners.[88,89]

Small negative Poission's ratios have been observed naturally in, for example, metals,[90] polymers,[91,92] and silica.[93] Besides these bulk materials, Lake *et al.*[94,95] produced artificial 3D auxetic materials from conventional low-density open-cell polymer foams by heating, then crushing the foam and cooling below the foam's glass transition temperature (T_g) causing the ribs of each cell to permanently protrude inward. Subsequent external tension applied to vertical elements in the re-entrant foam structures caused the modified cells to unfold and expand laterally. A Poisson's ratio of -0.7 was observed at a small tensile strain (less than 0.02), then gradually decreased, but remained negative up to a strain of 1.3. Even though an artificial auxetic material was demonstrated with these macroscopic foams, similar phenomena can be expected in the micro- and nano-scale with improved performance due to the ability to rationally design a periodic material.

To date several methods have been tried to create auxetic materials in a well-controlled manner instead of the stochastic one; for example, Xu *et al.* used soft lithography to fabricate various 2D MNSMs to exhibit auxetic behaviors at the micron-scale as shown in **Figure 12**.[96,97] These 2D MNSMs only show auxetic behavior for in-plane strains in a highly anisotropic fashion; however, they are still valuable for certain applications in microelectromechanical systems (MEMS).[98] As theory predicts, a large number of MNSMs can show auxetic behavior,[99] it is quite likely that more 3D auxetic MNSMs will be demonstrated with the advance of fabrication techniques and identified applications.

Even though many natural crystals have been identified as 3D auxetic materials,[90,100,101] it has been a challenge to design 3D auxetic MNSMs. Gaspar *et al.* tried to design a macroscale 3D model of a periodic structure made of tetragonal nodules interconnected by rod-shaped elements.[102] Pikhitsa *et al.* presented a model for the three-dimensional auxetic material, which deals with individual multipod constituents arranged in a lattice. The model was experimentally verified with a macroscale ball-and-stick construction.[103] In addition, certain truss structures inspired by cubic bulk auxetics that consist of a network of bending beams have been numerically shown to exhibit auxetic behavior for a specific crystalline direction.[104] Recently Bückmann *et al.* experimentally demonstrated 3D MNSMs having a uniaxial auxetic behavior at the micron-scale.[105] As seen in **Figure 13**a, unit cells of the structures designed by 4-fold rotations of the 2D auxetic structures shown in Figure 12b demonstrate negative Poisson's ratio $\nu \sim -0.12$ up to a strain of 10%. By choosing different angles of tilted elements, values near zero and positive Poisson's ratios are also possible.

It is often overlooked for auxetic properties that the actual effects have typically only been exhibited in the limit of small strains (<10%). Indeed, Figure 13d and 13e show the strain-dependence of auxetic behavior. Since current examples of the auxetics only show the effect in the limit of small strains, persistency to large strain should be considered in design of MNSMs. Moreover, efforts to increase the maximum working strain and strain rate are valuable for certain applications such as mechanical energy absorbers. Further, at these larger, plastic strains, architectures that would not be expected to show auxetic behavior may demonstrate negative Poisson effects, such as has been shown in simulations of biomimetic hierarchical ordered composites.[106]

2.6. Improving High Strain Rate (HSR) Mechanical Behavior

When materials undergo HSR deformation such as caused by blast or ballistic impacts, large nonlinearity and complex inelastic deformation mechanisms are present. Strain rates above 10^2 s^{-1} are classified as high strain rates, strain rates above 10^4 s^{-1}, very high strain rates, and strain rates above 10^6 s^{-1}, ultra high strain rates. HSR phenomena have been extensively studied in a broad range of polymers,[107] metals,[108] and ceramics;[109] however, the HSR behavior of materials is still relatively poorly understood. Recently nanomaterials have been utilized as convenient model systems–for example, strain rate dependent deformation of nanowires,[110,111] HSR damage

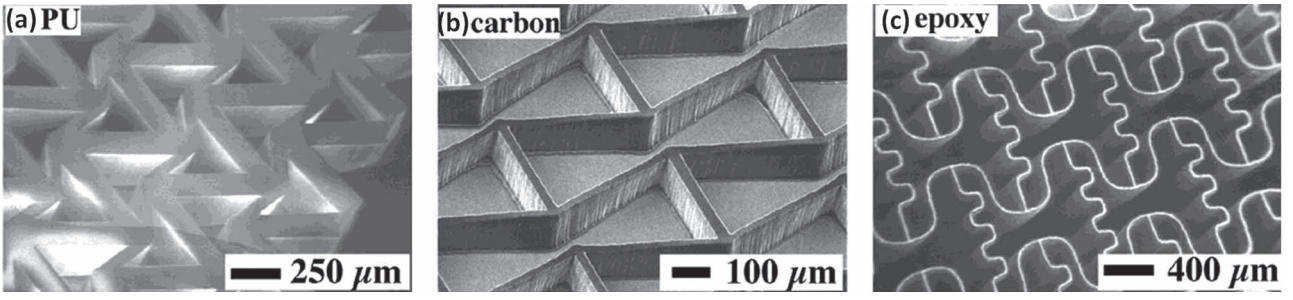

Figure 12. SEM images of 2D auxetic MNSMs made from various materials: (a) polyurethane (b) glassy carbon (c) epoxy. Reproduced with permission.[96]

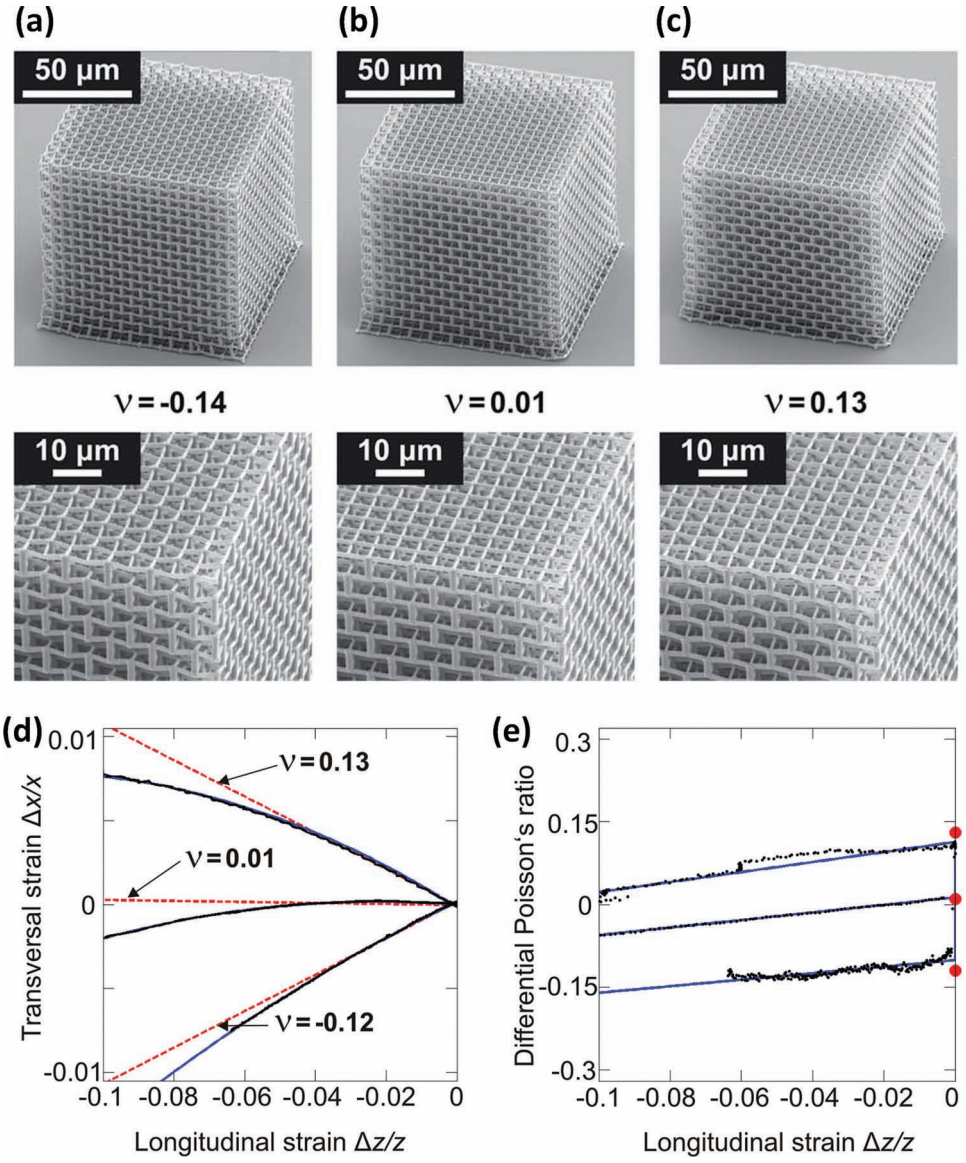

Figure 13. SEM images of MNSMs having (a) negative, (b) near zero, and (c) positive Poisson's ratio. (d) Measured transverse strain curves of the three MNSMs as a function of longitudinal strain are plotted along with their initial slopes (red dashed lines). (e) Differential Poisson's ratio as a function of longitudinal strain for the three MNSMs. The red dots are the initial Poisson's ratio, which is a slope of the red dashed lines in (d). Reproduced with permission.[105]

mechanisms of multiwalled carbon nanotube,[112,113] and HSR deformation mechanisms of nacre's aragonite plate.[114] As mentioned in the previous sections of this article, the various mechanical characteristics of MNSMs are primarily based on quasi-static deformation or vibration in the elastic regime; thus, HSR characteristics of MNSMs are virtually a new topic of materials science. Of course, for quasi-static deformation, all mass elements respond to the stress at equilibrium. As the strain rate becomes high, every mass element is not in equilibrium because the internal stresses are not instantaneously transmitted, but rather do so at a finite speed. As a result, the response of a material at HSR tends to be determined by its local characteristics. Consequently, the fundamental understanding and rational design of materials at the micro- and nano-scales is crucial in order to improve HSR performance. Since the structural scale of MNSMs can be sufficiently small to exhibit the length scale dependent effects at HSR deformation, the assessment of the MNSMs at HSR is also important to exploit new physical phenomena.

The principle challenge for the study of HSR behavior is the lack of a versatile and efficient set of test methods to investigate small-scale mechanical deformation and failure mechanisms at HSR and to high strains. One promising approach is microscopic ballistic testing, since the sample size and the deformation volume can be significantly reduced. The reduced deformation volume is advantageous in both sample preparation and characterization. More than a half century ago, Shelton *et al.* demonstrated a micro-ballistic test conducted under vacuum

with small metallic particles by use of an electrostatic accelerator to reach velocities in the range of 1–3 km/s.[115] This approach has been developed to achieve higher velocities up to 80 km/s to simulate a micrometeoroid impact.[116] Another method is the laser-driven flyer (LDF) technique, where high-speed, small objects can be launched by a pulsed laser to impact a target specimen.[117,118] In LDF, a metal thin film (usually aluminum) is deposited on a transparent substrate, and a short (few ns) laser pulse is aimed at the thin film. A high-pressure and high-temperature plasma is created by a partial ablation of the thin film and causes the spalled layer to accelerate, which results in an impactor flying away from the substrate at a velocity of a few km/s. Compared to electrostatic acceleration, LDF is a technically simpler method to create high speed projectiles, but the shape of the projectiles is irregular due to the method of their creation. Instead of direct ablation of the flyer material, a flyer can be deposited on a laser absorbing film to be ablated in the laser induced forward transfer (LIFT) technique. Thus, the actual flyer can be nearly undamaged even for thermally and mechanically sensitive materials.[119] This method, however, is as yet not currently applied for HSR experiments, but rather as a fabrication technique for functional 2D structures.[120,121]

Recently we found that solid silica beads (~3.7 μm diameter) can be similarly accelerated to several km/s by use of a laser pulse and then impacted to a specimen to mimic a macroscopic ballistic test. **Figure 14** displays impact features of three different materials: a polycrystalline aluminum film, a stochastic nano-composite (hollow silica beads/PMMA), and a periodic polymer/air MNSM. A valuable characterization method is cross-sectioning of an impact site using focused ion beam (FIB) milling. The back-scattered electron image of the deformed aluminum after ion-beam milling (Figure 14d) reveals changes in grain shape as well as the appearance of shear bands in the target metallic material. There are also unique high strain rate features in the hollow silica beads/PMMA target sample (Figure 14e). During the impact, the hollow silica bead/PMMA composite is densified by sequential collapse events of the hollow spheres, which should lead to strong nonlinearity in the deformation and the potential for a new lightweight, high-performance protective material. In contrast, the epoxy/air MNSM (Figure 14f) is substantially deformed in the lateral directions (evident by comparing the size of the crater to the sphere diameter) due to the ability of the framework to laterally distribute the stress through diagonal struts. This nonlocalization of impact damage will help to stop projectiles in shorter distances by engaging more material without increasing target thickness. Note the extreme deformation of the silica projectile in Figure 14d, which suggests study of the deformation behavior of the various projectiles is also possible.

2.8. Smart Materials Using MNSMs

Since the characteristic behaviors of MNSM based devices arise from the physical geometries and materials parameters, it is interesting to address the dynamic mechanical parameters for actively tunable "smart" structures. Field responsive piezoelectric and magnetostrictive materials, which undergo strain under applied electronic and magnetic fields, are one group of materials that have been investigated. In the kHz range, tuning of phononic bandgap of a 1D composite metal-piezo system has been studied.[122,123] It was shown that not only could the positions of existing stop-bands be tuned, but also new gaps could be introduced of a magnitude of $\Delta\omega/\omega \approx 0.1$. These results, however, required the application of piezo-excitation at frequencies commensurate to the band position, which are increasingly difficult to achieve as MSNM devices are approached. Magnetostrictive phononics has also been investigated theoretically for

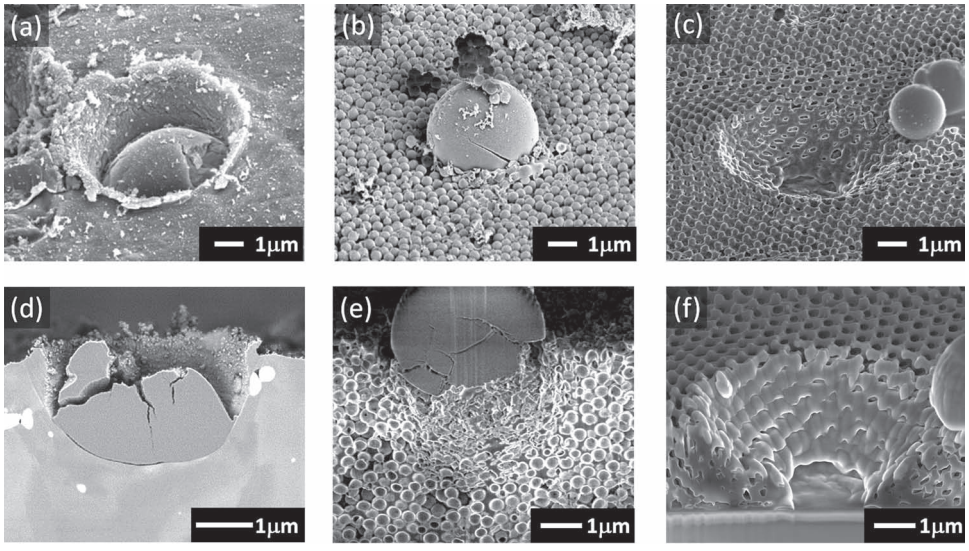

Figure 14. Deformation features of various materials after impact in the laser-induced projectile impact tests. (a) Aluminum film (b) hollow silica/PMMA composite (c) epoxy/air MNSM. Back scattered electron micrographs of a cross section of an impact site in the (d) polycrystalline aluminum film (e) hollow silica sphere/PMMA composite (f) epoxy/air MNSM.

2D phononic crystals.[124] In this study, a square array of ferromagnetic blocks in a polymer matrix were shown to have a tunable band structure under a static magnetic field, both by widening (~40% increase of the first gap) and also by closing bandgaps for potential switching. Both of these field tuning mechanisms, however, tend to have relatively weak coupling, requiring high fields for tuning.

Another potential mechanism for dynamic MNSM metamaterials is use of a thermally induced phase change. During a transition between two phases, the mechanical properties can vary a great deal in both their magnitude, and also their anisotropy (e.g. switching between two crystal states or, for example, from an anisotropic crystal to an isotropic liquid). Such phase changes have been investigated for phononic systems. Sato *et al*. studied a system of a hexagonal array of pores in anodized aluminum oxide (AAO) filled with a polymer.[125] When the polymer was put through its glass transition (a drop of ~10^3 in elastic modulus between the glassy and rubbery state), the impedance contrast between the holes and the matrix dramatically increased, leading to altered dispersion in both the in-plane and out of plane modes. The thermal tuning of a ferroelectric phononic crystal by phase transformation has also been investigated.[126,127] In these theoretical studies ferroelectric blocks or disks in an epoxy matrix were predicted to show changes in their band widths (increase in main band by ~10-20%) and positions of higher bands with only moderate changes in temperature. Indeed, the change in the upper band position of up to ~15% have been demonstrated experimentally.[126]

The mechanisms detailed above are relatively subtle in their effect on selection of the overall geometrical shape of the structure. In contrast, polymeric gels can demonstrate large changes in both properties and sample dimensions. These systems are made from entangled or lightly crosslinked network polyelectrolyte polymers which can be highly swollen by an appropriate solvent. From the standpoint of metamaterials, swelling changes not only the size of the material, but also the other properties, such as optical index, density and modulus. While the former two properties only change slightly by swelling, elastic modulus can be significantly tuned over at least an order of magnitude.[128] This has already been successfully exploited to make tunable 1D photonic[129] and phononic crystals[130] by self-assembly and crosslinking of a diblock copolymer with a hydrogel block, allowing for tuning of the band properties by various stimuli (e.g., ionic strength, pH, and temperature). Gel patterning has also been applied to 2D and 3D phononics such as the design of stretchable IL 3D phononic structures[131] and organic swelling effects to enable phononic pattern transformation in 2D IL systems.[132] In contrast to the studies above where the band structure was changed by altering the mechanical constants, it is important to note that the gel tuning changed also the *symmetry* of the phononic crystal, which significantly alters its anisotropy. For example, Jang *et al*. demonstrated the transformation of a p6mm, 2D epoxy structure to a lower symmetry, non-symmorphic, p2gg structure by substrate-confined swelling leading to stress-induced pattern instability.[132] This in turn forced avoiding mode crossings leading to the opening of a complete bandgap in a material which previously had only partial gaps. Further, the change in properties was accomplished without either a large field or a crystal phase transformation, and with only ~ 5% strain field, illustrating the power of non-affine transformations, such as pattern instabilities, to dramatically affect band structure and wave behavior. This is especially the case for high symmetry lattices such as the p6mm, where even uniaxial deformation has been shown theoretically to have a large effect on the band structure.[133] Elastomer fabrication has also been utilized in non-phononic mechanical metamaterials made by 3D techniques in the form of microactuators from microprojection stereolithography[134] and 3D direct write.[135,136] The only drawback of gel systems is that they require solvents, which can be undesirable for many applications.

One class of systems that has yet to be applied to MNSM, but shares some of the advantages of both the field tunable and gel systems are liquid crystalline elastomeric polymers (LCP). LCPs containing azobenzene side chain liquid crystals have been demonstrated as effective light driven actuators.[137–141] These materials go through a molecular level version of bimetallic strip bending due to either UV-induced structural shift in the LC group[140,141] or reorientation of the group to the polarization of blue-green light.[137–139] In the former case, a second exposure by visible light is required to reverse the transformation, while the latter can occur so rapidly as to drive oscillations.[137] Either of these mechanisms could have interesting effects if applied to MNSM mechanical metamaterials, however, there may be some scaling considerations due to the surface strain-induced effect.

3. Fabrication

Many demonstrations of the MNSMs have utilized macroscale fabrication techniques such as machining or other "handmade" techniques;[48,49,54,55,142,143] however, for the development of many devices it is necessary to utilize micro or nanofabrication techniques. It is important to note that many structures that have been fabricated to investigate other physical effects could have applications as mechanical metamaterials, but have just not yet been analyzed. An obvious example is photonic crystal structures, which, without exception due to the higher-mechanical-than-optical contrast of most materials, could also be utilized for phononics. For this reason, it is important to consider fabrication techniques that have not yet been directly applied to the MNSMs, especially in 3D fabrication, where the varieties of possible techniques are rapidly increasing.

In transitioning a technique from one application area to another, one needs to consider what materials parameters and tolerances are present. For example, complementary metal-oxide-semiconductor (CMOS) devices require a high degree of control in both the purity and the roughness of the fabricated devices to attain the required function. The same can be said for photonic systems, where the greatest possible index contrast exists within an order of magnitude from vacuum, making composition critical at times, and roughness can lead to radiative losses. While the same can be said in the latter case for phononic crystals, the massive contrast between for example, a metal ($Z \sim 10^6$ kg·s/m^2) and air ($Z \sim 4 \times 10^2$ kg·s/m^2) leads to a relatively high tolerance to variations in composition or relative porosity. Further, in the case of more classical mechanical metamaterials, such as auxetics, roughness and even relative positioning is relatively unimportant, as long as the connectivity

and critical geometric features (such as re-entrant structures) are preserved. An important exception to the reduced sensitivity is the HSR response of MNSM, where modes of brittle failure can be initiated and propagated by single flaws leading to catastrophic failure.

3.1. 2D Fabrication

Much of the current work to date on mechanical metamaterials has been conducted on 2D systems, especially in the areas of phononics and auxetics. As the requirements for mechanical devices are more flexible than optical, there is a wide range of materials and techniques that can be utilized. Microstructured auxetics have been made by microstamp and embossing techniques.[96] In these studies an optically patterned master is utilized to imprint the desired structure into a soft material, which can then be either used as the final product or inverted into another material by, for example, electroplating, or controllably combusted into amorphous carbon. High power pulse laser ablation has also been used to create 2D auxetic materials by employing high power pulse lasers to directly micromachine polymer structures.[83] For studies of 2D phononic devices, high resolution phononic structures and actuation resonators were patterned with submicron feature sizes.[44,144–146] To accomplish this, conventional CMOS techniques of patterning with optical lithography and subsequent etching were employed.

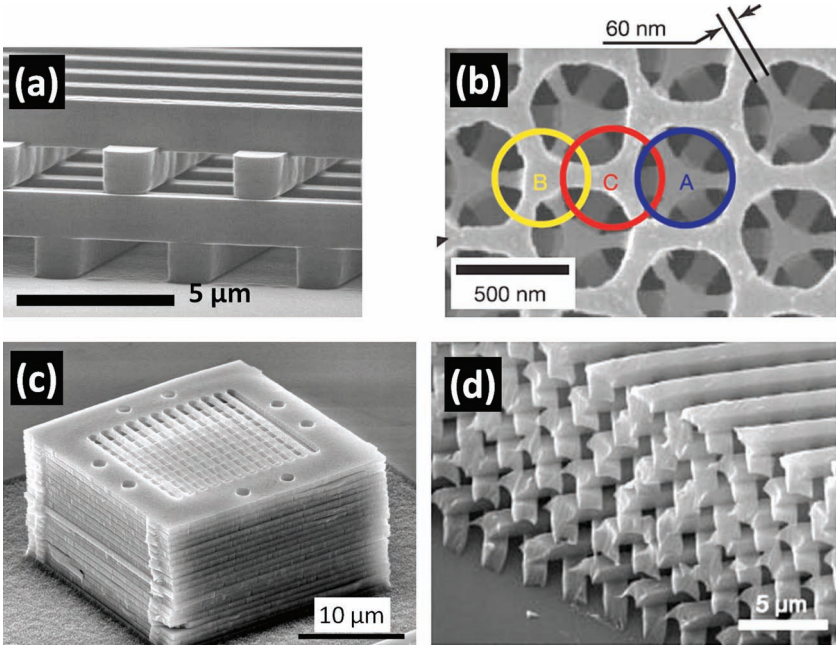

Figure 15. Layer-by-layer fabrication. (a)-(b) silicon photonic crystals by conventional photolithography. Reproduced with permission.[148–149] Copyright 1998, 2004 Nature (c) Photonic crystal by stacking of 2D indium phosphide plates. Reproduced with permission.[151] Copyright 2003 Nature. (d) Polymer structure by soft lithography. Reproduced with permission.[150]

3.2. Layer-by-layer Fabrication Techniques

Micro and nanoscale mechanical (much as the analogous optical) metamaterials require a different set of process capabilities to design many of the features necessary for 3D devices. It is possible to accomplish fabrication of 3D structures by the layer-by-layer stacking of multiple 2D structures.[147–150] These fabrication methods have been performed in the past for photonic devices. The layer-by-layer techniques can be divided into two approaches, subtractive and additive ones. In the subtractive approach, each 2D structure is defined by etching, for example, a 3D periodic silicon structure has been produced by the iteration of 2D structural patterning sequences consisting of silicon deposition, masking, etching, sacrificial material deposition, and chemical-mechanical planarization (see **Figure 15**a and 15b).[148,149] In spite of superior structural fidelity, the multiple steps make this approach costly and time consuming.

In contrast, in the additive approach, a pre-patterned 2D structure is simply added on top of the other 2D structure. Thereby, etching and related processes, sacrificial material deposition and planarization can be eliminated. For example, 3D structures have been made by stacking multiple grating structures using micromanipulation.[151] In this work (Figure 15c), simple 2D semiconductor processing was used to make individual 2D semiconductor structures that were positioned in stacks of the desired functionality. Since the free-standing 2D structure is nothing but a patterned thin membrane, this approach may be difficult to apply for a wide area 3D structure due to the mechanical instability. A full-additive approach without any etching was done by layer-by-layer transfer of polymer structures carried by an elastomeric substrate (Figure 15d).[147,150] The soft lithographic techniques are attractive for wide sample size, low cost, and high structural fidelity.[77]

All the layer-by-layer techniques, however, have significant limitation on aspects such as features that cross multiple levels, the ability to have multiple material types in close proximity at the same height, and loss of resolution/precision due to registry and layer-to-layer mechanical integrity and stability considerations. As research into conventional lithography alternatives progresses, the variety of techniques for creating complex 3D assemblies is ever increasing, along with the variety of possible structures and the degrees of available tunability.

3.3. Angled Exposure Techniques

One of the strategies for the generation of 3D structures involves the application of conventional top down techniques with the added feature of the use of multiple angles. Among the earliest of these techniques is glancing angle deposition (GAD),[152–155] in which a seeded or bare substrate is exposed to an evaporated source at an angle near 90° (**Figure 16**a). By adjusting the rotation of the substrate with respect to the source, the direction of growth can be controlled. Initially, this was restricted to angling of grains in thin films; however, it has been expanded to the

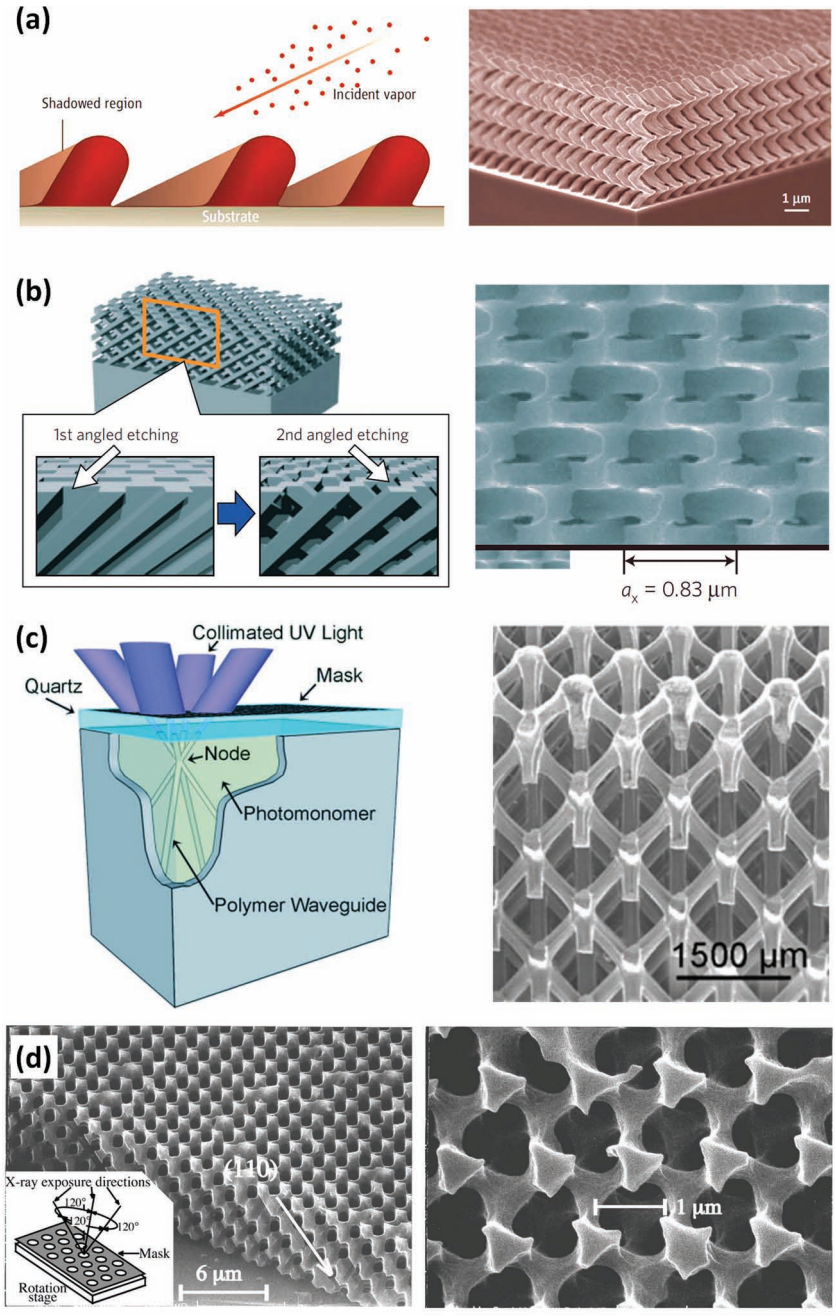

Figure 16. Schematics and SEM images of the MNSMs produced by angled deposition methods. (a) Spiral structures fabricated by GAD. Reproduced with permission.[156] Copyright 2008 Science. (b) Woodpile-like structures produced by angled reactive ion etching. Reproduced with permission.[157] Copyright 2009 Nature (c) Ultra low density mechanical microframes produced by SPPW. Reproduced with permission.[158] (d) f.c.c.-like nanoframes produced by X-ray lithography. Reproduced with permission.[159] Copyright 2000 American Institute of Physics.

generation of high aspect ratio helices with nanoscale diameters and pitches.[153,154]

Another set of angled techniques feature exposure through a 2D physical mask. In angled etching (Figure 16b),[157,160,161] a metallic mask patterned by conventional 2D lithographic techniques is utilized as a barrier for a reactive ion etch. In this way angled holes can be directed through a semiconductor to form a 3D pattern potentially containing line defects.[157] An analogous soft lithographic technique that has been applied to mechanical metamaterials is self-propagating polymer waveguides (SPPW)[27,158,162] (see Figure 16c). In SPPW, a physical mask is placed on top of a liquid polymer photoresist that is exposed to angled, collimated UV light. The resist is selected to exhibit a significant increase in index upon crosslinking such that the propagation of the exposing light is waveguided through the resist, including through intersections (or nodes) of two waveguided beams. The net result is the highly robust fabrication of 3D polymeric truss structures down to the micron scale which can be used as templates for generation of elastomeric or metallic filled or hollow structures by coating or double inversion.

SPPW becomes inefficient when the feature size of the mask is comparable to the wavelength of UV light due to severe diffraction effects. X-ray lithography[159] (Figure 16d) is an alternative to circumvent the diffraction issue by virtue of its significantly shorter wavelength. A metal mask is placed on an X-ray sensitive polymer layer and consecutive exposures to a highly directional x-ray beam such as synchrotron radiation are performed at different angles. The area exposed above the critical dose can then be dissolved during development. Although the resultant structure is similar to that from SPPW, the definition of elements does not rely on the waveguiding but rather on simple projection.

3.4. Interference Lithography

The phenomenon behind interference lithography (IL) is the formation of non-uniform intensity fields by the interference of two or more light sources of different directions, polarizations, amplitudes, and/or phases. At the zone of coincidence of the sources, the interference patterns will be periodic or quasiperiodic with periodicity determined by the above parameters along with the wavelength(s) of the sources. By locating the resulting interferogram of properly tuned light sources inside of a photoresist, the interference pattern can be converted into a 1D, 2D, or 3D structure by a change in chemical functionality, (de)crosslinking, or (de)polymerization reaction of the negative(positive)-tone photoresist. The two general strategies to accomplish IL are multi-beam and phase mask interference.

In multi-beam (MB) interference,[163] patterns are generated by the interference of multiple beams of selected intensity, polarization, angle of incidence, and phase, usually generated

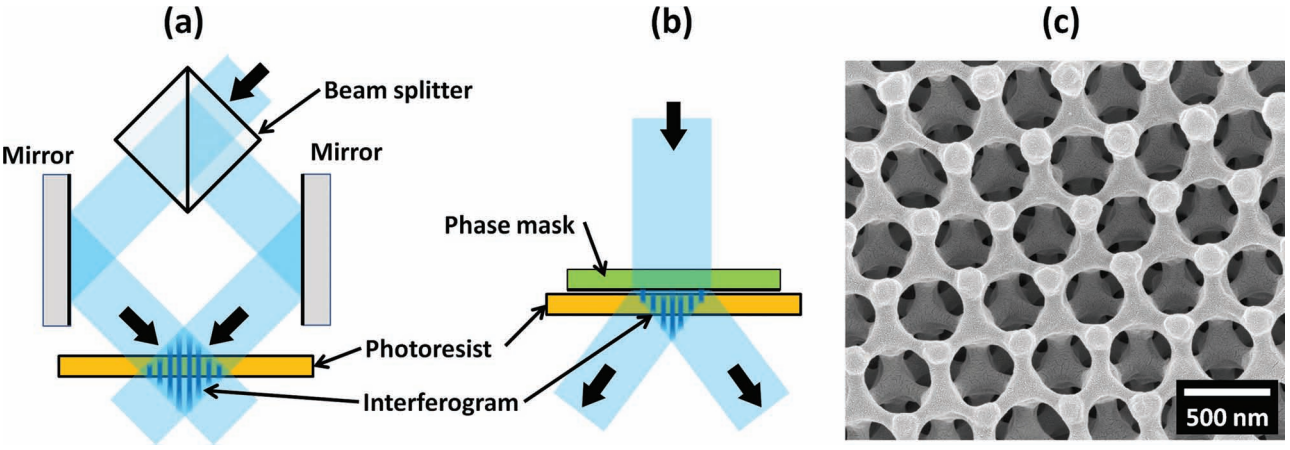

Figure 17. Schematic of (a) multi-beam interference lithography and (b) phase mask interference lithography. For simplicity only two beams are illustrated. (c) SEM image of a SU-8 photoresist structure fabricated by 4-beam interference lithography.

by a splitting of a coherent source such that the consideration of phase may be controlled purely by the relative path lengths of the various beams (**Figure 17**a). The greatest attraction of this approach is that it has a solvable inverse problem–with a target structure in mind, it is possible to determine the necessary beam parameters to achieve a structure approaching the target by solving a Fourier expansion of the desired intensity distribution.[41,164] In this way, MBIL has been utilized to fabricate phononic,[45,165] and mechanical structures,[24] as well as photonic structures.[166,167]

Phase mask interference lithography (PMIL) is a much simpler technique than MBIL. In this approach a phase mask is brought into contact (or deposited on via imprint[168] or self-assembly[169]) with a solid photoresist (Figure 17b). The mask, a 1D or 2D pattern (possibly in multiple layers[170]) is then used to produce multiple diffracted beams from a single incident beam, which in turn produce an interference pattern within the resist. Thereby, the phase mask (and generating master) are the only required optics (though practically there are some considerations for the light source) for generating complex, large area 3D patterns, and have been used for the generation of structured particles[171] and photonic crystal templates.[172,173]

Overall, MBIL is advantageous in the capabilities of non-contact exposure and a wider range of possible structures while PMIL is valuable for its simpler optics and resistance to environmental perturbation like mechanical vibration.

3.5. Direct Write Lithography and Printing

Direct write (DW) lithography is the most intuitive form of lithography and also provides the greatest degree of arbitrary control, as patterns are not restricted to a specific periodicity or characteristic length scale. For 3D structures there are a variety of printing and patterning processing techniques that are well suited for the production of metamaterials.

Nozzle based printing techniques are a versatile method for the rapid production of 3D structures that can be decomposed into vector maps. The most common example of such a technique is commercially available 3D printing tools. These use molten polymers or UV-curable polymers to write features on the sub-mm scale and have been employed for the characterization of the deformation properties of model system lattices prior to approaching MNSMs (**Figure 18**a).[32] Recently, a variation of this technique using functional sol-gel inks has been developed.[174–178] By utilizing shear thinning colloidal inks, structures of various materials, including polymers,[176] metals,[177] and semiconductors,[178] can be rapidly patterned down to the micron scale. This technique has been applied to structures ranging from photonic woodpiles[175] to vascular networks,[179] but has yet to have direct mechanical applications, though the potential is high.

A variation on nozzle 3D printing is layer-by-layer 3D printing. In this technique, the patterned media is introduced one layer at a time from the bottom up and progressively patterned. This has been accomplished both with granular media using a glue nozzle and also highly absorbing liquid photoresists. This latter technique, called microprojection stereolithography (Figure 18b),[181] allows for nearly arbitrary fabrication with micron scale resolution by slowly sinking the patterned structure in a resist bath and exposing the newly formed surface layer of resist to 2D UV light patterns controlled by a digital mirror array. The exposure light can only penetrate a small depth into the resist, thus defining the rate at which the structure can change. This technique has been utilized to design mechanically actuatable structures by patterning in a hydrogel resist.[134]

3D optical direct write by a focused laser beam is also a very popular fabrication method. In these techniques, nearly arbitrary patterns are "written" in a photoactive media by the patterning laser via either controlled motion of the relative position of the sample and lens or by deflection within the field of view by galvano-mirrors. While the earliest demonstrations utilized single photon absorption at the edges of the absorption band,[182] multi-photon lithography (MPL)[183–188] or other nonlinear effects[189–191] have become the standard methods for rapid patterning of nearly arbitrary 3D structures. MPL is performed

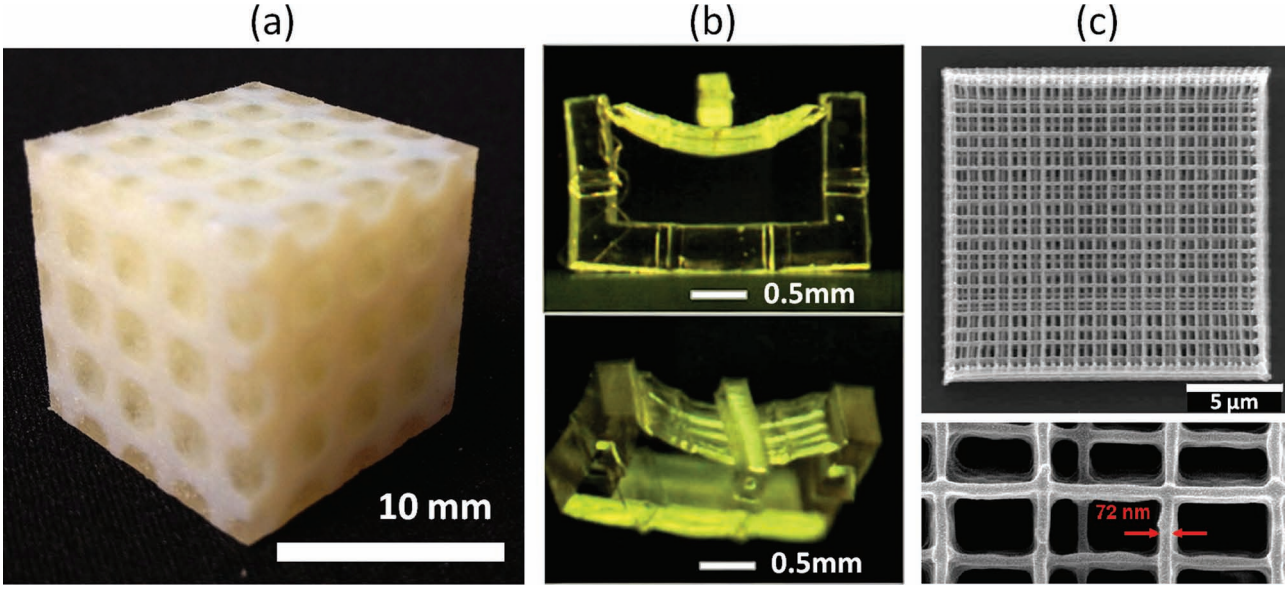

Figure 18. 3D fabrication by direct writing techniques. (a) 3D periodic structure created by mm scale 3D printing of polymeric bi-continuous structures at the mm scale. Courtesy of L. Wang at the Clarkson University. (b) Hydrogel actuator structure made by projection micro stereolithography. Reproduced with permission.[134] Copyright 2010 IOP Publishing. (c) High resolution MPL polymer patterning of a 3D structure with sub-100 nm resolution. Reproduced with permission.[180] Copyright 2007 Optical Society of America.

by the activation of a photoinitiated process by simultaneous (on the timescale of the excitation) multiple adsorptions of light below the absorption edge of the initiator. Most typically this is a UV excitation driven by double adsorption of visible or NIR light; however, three photon MPL has been demonstrated.[184]

The capability for 3D DW arises from this multiple adsorption process–the rate of a photoinitiated process will scale as the intensity to the power of the number of simultaneous adsorptions required,[187] thus increasing the resolution of the technique (See Figure 18c). MPL of photoresins currently has been primarily used for photonics[185] and plasmonics;[192] however, it has more recently been applied to mechanical metamaterials for fabrication of 3D auxetic[105] (see our earlier Figure 13) and previously unrealized so called, "pentamode structures" that can provide a very large ratio of the bulk modulus to the shear modulus (10^3–10^4) and hence act as a type of metafluid where there is very little coupling between compressional waves and shear waves.[193,194] Such pentamode materials could be utilized as building blocks for achieving almost any desired elasticity tensor. A more unique process to MPL is the direct photoreduction of dispersed metallic salts into metal features, either out of solution[195,196] or a polymer matrix.[197–199] While the applications of 3D metal writing have currently been restricted to optical[195,197,199] or electronic structures,[196] the potential of patterning arbitrary high density metallic structures within a soft matrix could be exceeding useful for the development of mechanical architectures, such as negative modulus structures.

3.6. Self-Assembly

Self-assembly is another powerful tool for 2D and 3D fabrication of MNSMs. In these bottom-up processes, the natural arrangement of a particular structure is built into the chemical or physical parameters of one or more building blocks. The families of materials that have been studied for self-assembly are too numerous to list, but two of the most successful that are highly relevant for the generation of controllable 3D architectures would be colloidal systems and block copolymers.

Colloidal crystals are assemblies of micro or nano-scale particles formed out of solution (**Figure 19**a and 19b). The composition of the particles can range from organic polymers[200] and bioparticles[201] to inorganic glasses,[202] metals,[203] or ceramics.[204] Secondary van der Waals interactions are the primary driving force for assembly. By utilizing either slow evaporation times or various other techniques such as electrophoresis,[202] crystals of very high quality over a large area (up to cm scale) can be obtained. Colloidal crystal arrays have been employed extensively for photonic structures,[200,201,204,205] phononic crystals[206,207] and energy dissipative structures.[208] One disadvantage to colloidal systems formed by the most commonly employed monodisperse spherical colloids is the fact that they generally all form in the same crystal structure (f.c.c., $Fm\bar{3}m$) and, thusly, all have the same filling fraction. This limitation has been overcome with a variety of strategies, such as using multiple particle sizes (also allowing for multiple functionalities with controlled positioning),[209,210] pattered substrates,[211] or adding coordinating functionality to the particles by DNA surface binding.[212–214] The net result is a huge increase in the possible number of colloidal crystal structures.

BCP self-assembly is another route to multidimensional MNSMs that has been the topic of a great deal of investigation.[215] For BCPs made of two or more varieties of immiscible polymers covalently joined end-to-end (or in more complicated architectures such as miktoarm star copolymers[216]), the BCPs undergo microphase separation resulting in microdomains with size commensurate to the relative block molecular weights and the period to the overall composition and total molecular

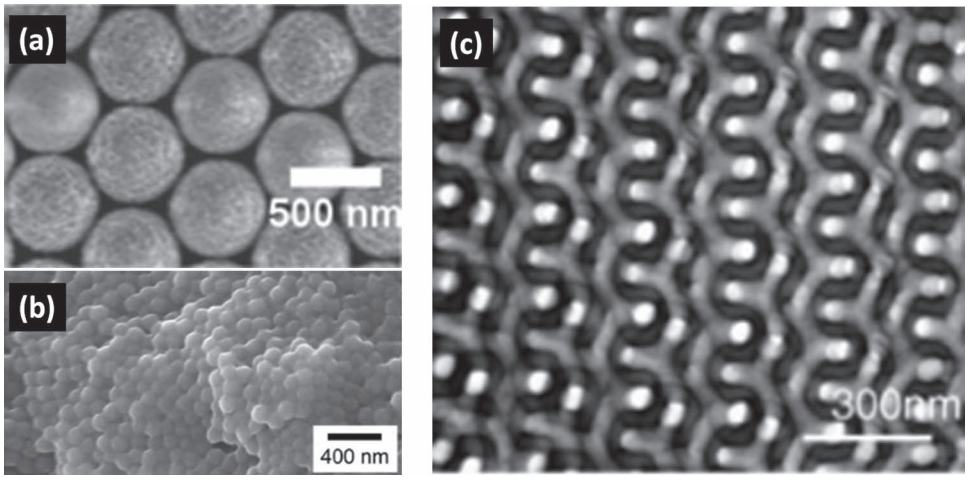

Figure 19. Self-assembled 3D structures. (a) 3D self-assembled polystyrene colloidal crystal in an f.c.c. structure. Reproduced with permission.[206] Copyright 2008 IOP Publishing. (b) Colloidal self-assembly of *Wiseana* viral capsids with an amorphous, liquid-like packing. Reproduced with permission.[201] (c) TEM image of double gyroid diblock copolymer self-assembly. Reproduced with permission.[63]

weight. The arrangement of these domains is dependent on the relative compositions of the individual blocks and the nature of their connection (architecture). For example, in the simplest case of a diblock copolymer, there exist four distinct phases (in order of decreasing fraction of the minority block): lamellae, double gyroids (Figure 19c) of the minority phase in a matrix of the majority, hexagonally packed minority cylinders, and BCC packing of minority spheres.[217] Structural variants of these phases may also be obtained by various means, such as the formation of a helical variant of the cylindrical phase due to a chemical choice of the backbone of the minority phase.[218] Additional symmetries are available by adding complexity to the block copolymer, such as by moving to a terblock,[219,220] leading to more than ten new distinct phases. Blending nanoparticles (NPs) into a BCP solution can also result in highly structured bi-composites due to the ability of the NPs to reside in low energy regions within the polymer medium, dictated by the geometry and scale of the block domains and the enthalpic interactions of ligands on the NP surfaces.[221,222] Applications of block copolymers include photonic[63,129] and phononic[223] crystals, which, by virtue of the soft nature of the BCPs can, by selective crosslinking and swelling, have their photonic and phononic dispersion tuned by a variety of stimuli.[129,224] Because bulk MNSMs formed from BCP can have periodicities ranging from 1 to 100 nm, their application to phonon-engineered materials is very promising.

3.7. Combined Approaches

All the techniques discussed above possess advantages and limitations. The most general areas of comparison for the various fabrication techniques are patterning rate, degree of structural control and resolution. These parameters are generally not completely independent. Most obviously, rate and control are generally inversely coupled. For example, the most rapid methods, such as techniques using single or multiple steps/exposures (imprint, photomask 2D lithography, glancing angle processes, microprojection, and IL) and self-assembly techniques can pattern a large area (mm-cm scale) in a single lithographic step. While layer-by-layer techniques fall into this category, most of them (other than microprojection lithography) when applied to 3D structures require many intermediate steps that slow down the process. The drawback of these techniques, especially in 3D, is that there is often very limited control over both the naturally occurring and desired defects. This is a particularly big problem in self-assembled structures that contain thermodynamic or kinetically frozen point or line defects. Conversely, IL structures can rapidly pattern a large area uniformly in 3D, but cannot controllably define point defects. In contrast, direct write techniques, such as 2D electron beam or laser ablation and 3D printing or MPL, can provide nearly arbitrary control over the structure with the limitation of serial writing. The rate at which these serial processes can occur is often coupled to the resolution of the process, with μm-mm scale direct write patternable at m/s rates, while fine MPL structures, writable down to a demonstrated 65 nm,[180] is generally limited to mm-cm/s depending on the simplicity of the patterned structure. Self-assembly is an exception to this rule; for example, BCP self-assembly techniques have the potential for the highest resolution as their characteristic length is limited by block molecular dimensions (1-100 nm) rather than optical or mechanical positioning and can pattern wide areas simultaneously with the drawback of the aforementioned defects.

These parametric tradeoffs have led to research into combined techniques. While these have generally not yet been applied to mechanical metamaterials; it is likely that hierarchically structured media produced by combined techniques will soon emerge in mechanical and phononic applications.

One example of combined techniques is the utilization of 3D direct write, usually by MPL, to introduce purposeful defects and create local hierarchical structures in 3D media patterned either by IL,[225–226] direct ink writing,[227] imprint,[136,228]

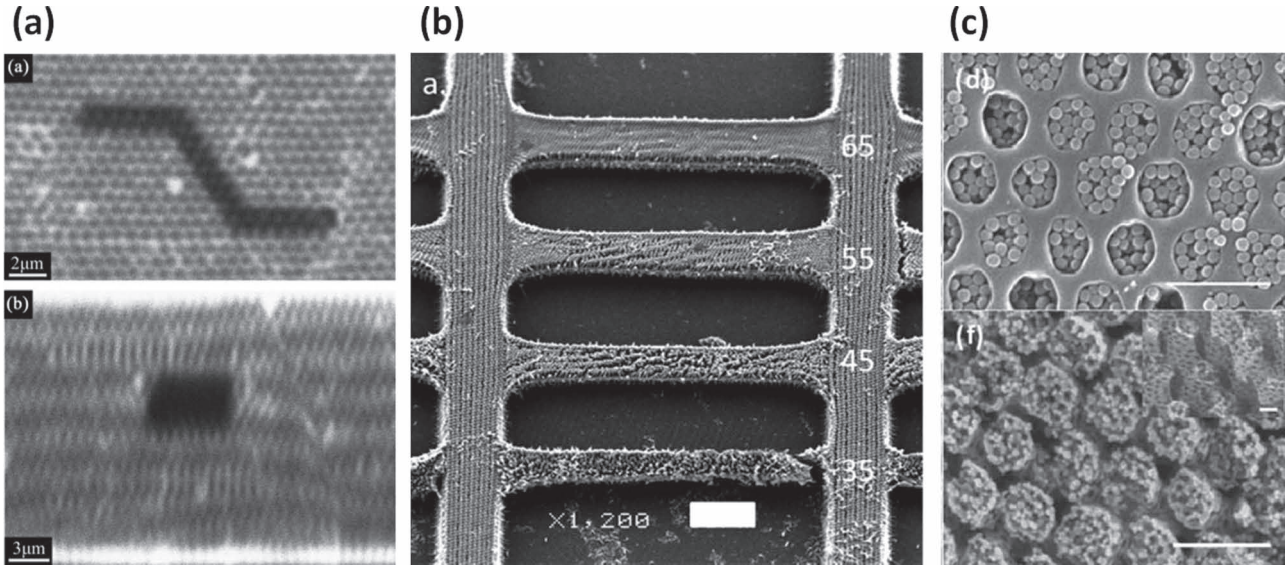

Figure 20. Examples of combined strategies for hierarchical 3D structures. (a) Confocal microscopy of a defect written by MPL within a colloid structure. The top image is a planar *xy* map of the defect, while the bottom shows a *yz* cross-section. Reproduced with permission.[232] (b) Locally patterned PMIL slabs with different fill fractions from a single UV exposure by focused laser spike (FLaSk) annealing with different powers of annealing laser. Powers (35-65) reported in mW. scale bar: 10 μm. Reproduced with permission.[225] Copyright 2011 The Royal Society of Chemistry. (c) Self-assembly of a fine colloidal structure in a MBIL pattern. The top image shows the initial structure, while the bottom shows a hierarchically porous inverted structure by titania sol gel. Scale bar: 1 μm. Reproduced with permission.[233]

or colloidal self-assembly[205,229,230](**Figure 20**a). In the case of the structures written on the imprinted pillars, micromechanical actuators were made by patterning in a hydrogel by MPL;[136] however, the other studies focused on optical devices. A similar approach has been made utilizing conventional short wave UV to fix a photocrosslinkable BCP that had been previously annealed for self-assembly;[231] the second block was then degraded to leave a fine featured hierarchical structure. In the above techniques, the fine structure was determined globally by the large area technique and then either altered or positioned by application of the second technique for a resultant binary product of either the 3D structure or fully filled/unpatterned area. More recently, focused laser spike anneal (FLaSk) has been utilized to generate hierarchically patterned structures with varying fill fraction from a single IL exposure by locally varying the bake conditions of a chemically amplified photoresist[225](Figure 20b).

Another possibility for technique combinations is the epitaxy of self-assembled structures. These techniques have been used extensively to guide the formation of BCPs in two dimensions by either chemical[234,235] or graphoepitaxy[236–238] to order and align the polymer microdomains. These are similar to unstructured, field-driven methods of BCP alignment, such as magnetic,[239] electronic,[240] mechanical,[241] thermal,[242–244] or directional solvent[245] evaporation or crystallization[246] driven alignment. Epitaxy of 3D self-assembly is a less studied area, though it has been demonstrated for colloids within conventional lithographic[233] or IL[247] templates (Figure 20c) and block copolymers within ordered and disordered pores.[248–250] Such structures could definitely possess interesting mechanical properties, but have yet to be analyzed with this in mind.

3.8. Methods for Material Conversion

Many of the processes detailed above are best suited for fabricating polymer/air based structures (furthermore, most often elastomer/air), which do not always possess the desired mechanical properties for a given application. For this reason, there has been a great deal of research on converting the initial polymeric structure to a different material. The most straightforward conversion method may be carbonization.[35,96] In this process, the polymeric structure is carbonized at a high temperature in inert environment or in vacuum. As a result, the polymer is converted into denser material (amorphous carbon), and elastic modulus is increased significantly. This converted material, however, is generally very brittle and the transformation also results in a degree of shrinking, potentially leading to crack formation. Very recently, this technique has been improved by absorbing the carbonized structure onto a metal layer deposited after carbonization, which in turn led to complete conversion to sp^2-coordinated hollow graphite.[251] One can also reduce the crack formation in carbonization by using a shrinkable substrate. For example, no observable cracks are found when we fabricate a SU-8 MNSM on a crosslinked SU-8 film and carbonize.

Inversion methods are perhaps the most commonly employed routes to create patterns in other materials. In these approaches, a material with the desired characteristics is backfilled into the internal space of a template and then the template is generally removed, though it may be left behind to generate bicontinuous solid/solid structures.[32] For example, a 3D photoresist template can be infiltrated with an elastomer resin and dissolved after crosslinking of the elastomer to leave a stretchable MNSM.[165] As a general process, inversions are executed through a variety

of methods in either direction between polymer and silica, with the final step of conversion to some final polymer, oxide, metal, or semiconductor. The reason for this is ease of removal–polymers can generally be dissolved by solvent or burned out by plasma etching while silica can be easily selectively etched by hydrofluoric acid. These methods were first developed in detail for silica and polymer colloidal crystals,[252–253] where silica and other oxides were deposited by the use of sol gel surface reduction of metal oxide compounds (such as shown in Figure 20c). This process could also be completed partially to create hollow or multilayered structures and was later applied to BCP[64] and IL[254] structures (with electrochemical assistance), though these structures often are somewhat porous due to difficulties in infiltration and often compact in a subsequent densification. For many applications, semiconductors such as silicon are the final target material due to their superior mechanical, thermal, and optical properties, but they can only be deposited by high temperature chemical vapor deposition (CVD). While this can be performed into silica colloids,[255] polymer systems are generally not stable enough to survive to the temperatures required. One way around this is to deposit a protective layer of either silica by low temperature CVD[175,256] and/or alumina by atomic layer deposition.[205,230,256]

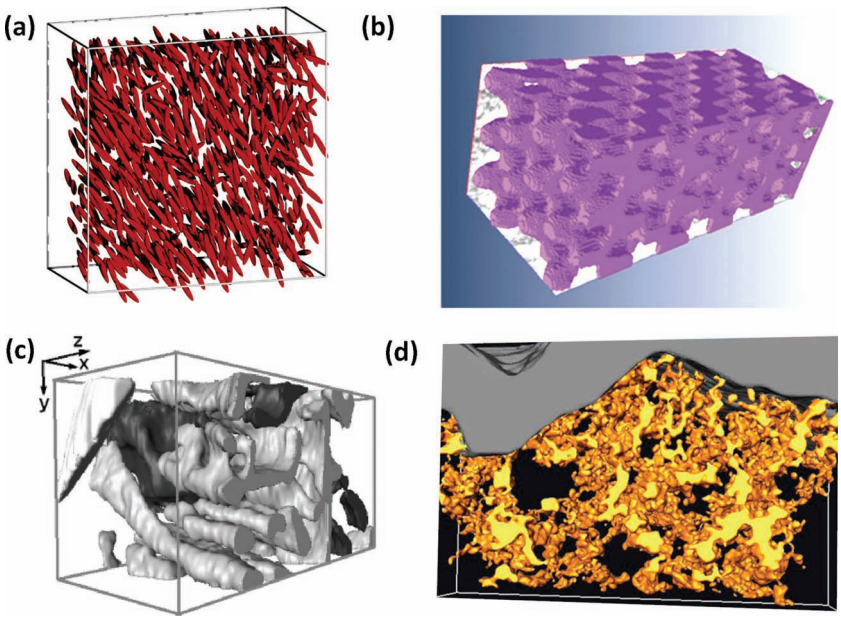

Figure 21. 3D structural images created by various imaging techniques. (a) Optical confocal microscopy (19 μm × 19 μm × 8 μm) of dispersed poly methyl methacryate (PMMA) ellipsoidal domains containing florescent dye in a polydimethylsiloxane (PDMS) matrix using florescence contrast. Reproduced with permission.[260] Copyright 2005 American Chemical Society (b) X-ray tomography (2.7 μm × 3.1 μm × 7.3 μm) of a HfO_2-coated SU-8 epoxy photonic crystal. Reproduced with permission.[263] Copyright 2006 American Institute of Physics (c) FIB tomography (14 μm × 8 μm × 7 μm) of $AlSi_8Mg_5$ alloy (aluminum phase is transparent). Reproduced with permission.[267] (d) TEM tomography (300nm × 200 nm × 100 nm) of ZnO (yellow) in conductive polymer (transparent) for a solar cell device. Reproduced with permission.[268] Copyright 2009 Nature.

Electrodeposition is a particularly versatile technique when 3D MNSMs are required. A non-conducting template is formed on a conducting substrate and target materials including oxide precursors,[254] semiconductors,[257] and metals[77,192] start to fill the electrolyte-filled internal space from the bottom (i.e. the electrode substrate) unlike other vapor phase deposition techniques. By removal of the template by a simple calcination or various etching techniques, inverted structures are achieved. A variant of this technique is electroless plating of nickel, in which an autocatalytic process leads to nearly uniform conformal deposition of nickel, which can be then etched out to make hollow structures as have been used for the ultra-low density, high modulus truss materials discussed above.[27] Metal coated structures can also be made by multidirectional sputtering, though this is subject to shadowing effects and thus is a less reliable technique.[228,258]

4. Selected Characterization Methods for MNSMs

4.1. Structural Characterization

Knowledge of the geometrical, structural, and compositional parameters of a MNSM is very important for accurate correlation with modeling. Although scanning electron microscopy is the generally employed standard for structural characterization, because of a broad range of materials, sizes, and 2D and 3D architectures, the measurement and parameterization of MNSM morphological characteristics are not easily accomplished by these surface-deep characterization tools. In this section, we introduce several techniques that are effective for the full geometrical characterization of MNSM.

Confocal microscopy (**Figure 21**a) is a powerful optical imaging technique for direct visualization of transparent 3D structures of material because of its high spatial resolution, especially in the axial direction.[259] In this technique, pinhole optics with a laser probe is utilized to enhance the contrast between various regions of varying composition produced by florescence[260–261] or refractive index.[129,165] In this way 3D imaging with sub-micron resolution is possible. X-ray tomography (Figure 21b) can provide another option for 3D structural information with the additional capability of being applicable to optically opaque samples. In X-ray tomography, tightly focused X-rays are used to probe the specimen and an X-ray camera is used to record the X-ray transmission radiograph. A set of radiographs are processed with a reconstruction algorithm to generate the tomogram of the specimen.[262,263] Because most materials for the MNSMs are optically opaque, X-ray tomography is frequently employed method for characterization of 3D microstructures.[264–266]

3D-TEM tomography (Figure 21d) enables the characterization of structures at nanometer-scale resolution[269] and has been applied to study solar cells,[268] terblock copolymers,[270] and semiconductor nanowires.[271] Although 3D-TEM tomography

itself is non-destructive, the preparation of specimen for the 3D-TEM tomography can be destructive in order to achieve the appropriate thickness of specimen necessary to allow electron transmission, which can vary depending on the acceleration voltage and sample electron density, but is generally in the sub-micron scale. Recent development of dual beam FIB/SEM instruments has enabled unique 3D material characterization through serial sectioning followed by high resolution SEM, electron backscatter diffraction, and energy dispersive spectroscopy (Figure 21c).[272] Consequently, combined FIB/X (where X = SEM, EBD and EDS) tomography can also provide volumetric information on structure and chemical composition as well, but at the cost of sample destruction.[267,273]

Unlike the previous tomography techniques, scanning acoustic microscopy (SAM),[274] enables one to obtain 3D structural information by directly probing mechanical properties if sufficient contrast exists in mechanical impedance of constituent materials (see Equation (5)). In SAM, focused longitudinal acoustic waves are transmitted to a sample in an immersion fluid and acoustic waves reflected at various internal interfaces of materials having different mechanical impedances are probed generally at the micron and supermicron scale. Using the phase, intensity, and time of flight of the reflected waves acquired during 3D raster scanning of the focused acoustic waves, a 3D mechanical map can be reconstructed. Because SAM is very sensitive to mechanical irregularity, it has been used for voids,[275–277] dewetting,[278] and strain fields,[277] multilayered polymeric systems[277] as well as quality control of semiconductor devices.[278–279] In addition, SAM has been utilized as a non-intrusive technique to examine the formation and healing of voids of self-healing composite of shape memory polymers, hollow SiO_2 glass particles, and carbon nanotubes under low strain rate impacts.[275] SAM has not yet been applied to multidimensional MNSM, most likely due to a combination of the technique's resolution and the difficulty of accounting for the multiple angles and complex paths of focused beams inside of metamaterials; however, there is likely some potential for SAM as a complimentary, non-destructive technique for probing dispersion properties of effective media MNSM, especially in geometries where scattering methods are impractical or opaque materials or encapsulated structures are required.

4.2. Nanoindentation

For mechanical characterization of modulus and yield, nanoindentation is one of the most common tools, which is simply an indentation test using submicron indenters. The principal goal of a nanoindentation test is to extract elastic modulus and hardness of a specimen material from experimental readings of the indenter load versus the depth of penetration. If plastic deformation occurs, then there is a residual impression left in the surface of the specimen. Unlike conventional indentation, the contact indentation area is often too small for direct measurement, thus the depth of penetration together with the known geometry of the indenter provides the indirect measure of the contact area at full load. Besides the modulus and hardness, the load-displacement curve often carries rich information for non-linear events such as phase transformations and cracking. The so called combined modulus, E^* is given by,[280]

$$E^* = \frac{1}{2}\frac{dP}{dh}\frac{\sqrt{\pi}}{\sqrt{A}} \tag{13}$$

where P, h, and A are the indenter load, the indentation depth, and contact area, respectively. In a typical test, load and depth of penetration are recorded as load is applied from zero to some maximum (loading curve) and then from maximum load back to zero (unloading curve). The material undergoes elastic and plastic compression during the loading and elastically recovers during the unloading. Therefore, dP/dh is determined from the unloading curve near the maximum load. The combined modulus is related to the actual elastic modulus (E) of the specimen and to the Poisson's ratios of the specimen and the indenter, ν and ν_I, and elastic modulus of the indenter (E_I) by the following equation.[281]

$$\frac{1}{E^*} = \frac{1-\nu^2}{E} + \frac{1-\nu_I^2}{E_I} \tag{14}$$

For a diamond indenter, because of its exceptionally high modulus (over 1,000 GPa), the second term may be negligible when testing specimens with moderate moduli. Residual indentation due to plastic deformation often shows the anisotropic nature of MNSMs. In **Figure 22**a it can be seen that the outline of the residual indent in the atomic force microscopy image is not circular but an equiangular 6-sided polygon although the polymeric MNSM was compressed by a spherical indenter. This reflects the 3-fold symmetry of the MNSM about the compression direction. Most indenters including spherical, Berkovich, Knoop, and Vickers create a localized stress field inducing elastic-plastic deformations, leading to a complex deformation response. Thus, a flat indenter may help to reduce the complexity by application of a more uniaxial-like stress distribution as seen in Figure 22b; however, it should be noted there are always edge effects near a perimeter of the indenter. Although edge effects can be lessened by using an indenter of a larger diameter, this approach requires increased parallelism between the specimen surface and the indenter. One of the ways to reduce the edge effect is FIB milling, which has recently become a popular method of sample preparation for compression analysis as discussed above. By use of FIB, a specimen can be shaped into a cylindrical form with a diameter smaller than the diameter of an indenter. Although ion damage during FIB should be taken into account, thus far ion-damage effects seem to be minor in the materials investigated.[30] If the MNSM is fabricated with an optically transparent material, Brillouin light scattering (BLS) can be an alternative method to analyze modulus due to its non-destructive nature and will be discussed later.

4.3. Optical Characterization

The use of optical and acoustic techniques for the measurement of mechanical properties is attractive due to the generally non-contact and non-destructive nature of the analysis. In

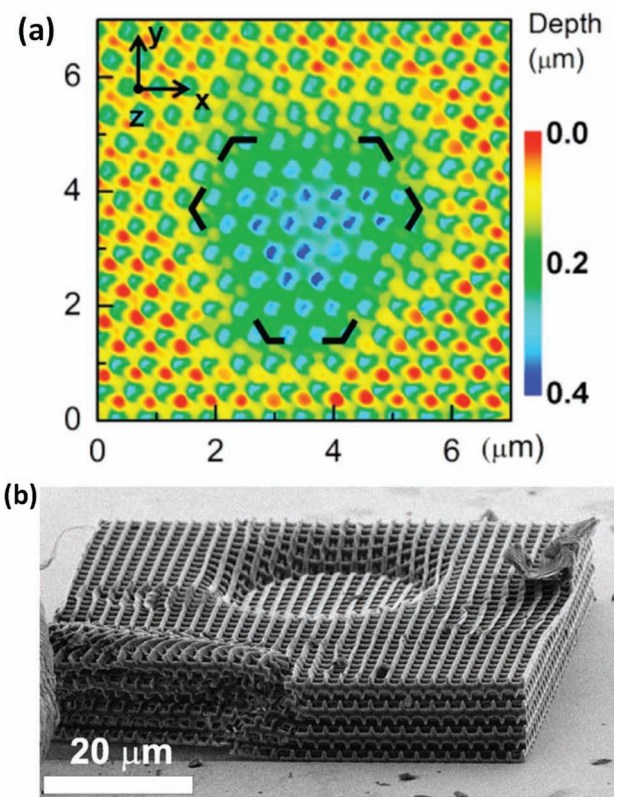

Figure 22. (a) AFM height image of the residual indentation after a 1.2 mN load applied for 10 s into an SU-8 epoxy MNSM. Reproduced with permission.[24] Copyright 2010 American Chemical Society. (b) SEM micrograph of a woodpile structure made of SU-8 epoxy fabricated on a glass substrate. The circular impression at the center is left by the flat punch during the tests that exceeded the elastic deformation limit. Reproduced with permission.[282] Copyright 2007 American Institute of Physics.

optical techniques, inelastic scattering processes of a photon with an acoustic phonon (Brillouin scattering) or with an optical phonon (Raman scattering) can provide a wealth of information about properties of materials. The acoustic phonon is represented by the vibration mode in which the displacement of an atom from its equilibrium position is in-phase with that of its nearest atoms, thus the change in bonding distance between atoms is very small. The bonding distance, however, is significantly stretched in the vibration mode representing the optical phonon due to the out-of-phase oscillation and associated energy level is higher (order of THz) than that of acoustic phonons (<500 GHz).

In a typical BLS setup, polarized light illuminates a sample and after scattering is then detected at a different angle and polarization. Based on the shift in energy of the scattered light at a particular angle, the wave vector of the interacting phonon propagating in this direction may be determined. The major challenge in the BLS technique comes from the very small energy shift. As the BLS peaks are very close to the several order stronger peak of the Rayleigh elastically scattered light, conventional spectrometers using dispersive elements such as a grating are not sufficiently effective to isolate the BLS signal from the central elastic scattering signal. Thus the spectral separation is accomplished by use of scanning Fabry-Pérot interferometer. Based on the incident polarization and the orientation of the sample, other properties such as components of the compliance tensor can be determined. Depending on the energy of the incident light employed, different length scales of the material can be probed. BLS is thus versatile at both determining bulk material parameters, such as the elastic constants of polymers,[283–284] or biological cells,[285–286] and for probing the dispersion relation of phononic metamaterials.[43,45] This was first demonstrated on colloidal crystals, where both the dispersion of the periodicity and the individual resonances of the particles were simultaneously probed[43,287] (the latter result may be considered Raman scattering). Phonons in such nanostructures possess energies in the GHz range, making it possible to resolve the frequency shifts utilizing conventional laboratory scale visible laser sources (frequency in the hundreds of THz); however, this also necessitates the use of index matching fluids in order to avoid conventional diffractive effects. In this way band structures for block copolymer phononic crystals[130,223,288] and even larger structures made by interference lithography[45,132,165,289] can be successfully studied.

Raman light scattering (RLS) probes light scattered by the optical phonons of a material corresponding to molecular vibrational states at the stationary "optical" limit (possessing crystal momentum near the Γ-point). RLS is sensitive to the degree of ordering in crystals,[290–291] resonances of quantum wells,[292–293] or the single particle vibrational modes of nanocrystals,[294] nanoparticles,[287] or nanotubes.[295] For many characterization studies, spatial mapping of the mechanical properties may be desirable. For this reason, Brillouin and Raman microscopy have been developed to characterize the local properties of either a mapped material[296–297] or a small object such as individual nanotubes,[298] and even 3D mechanical imaging.[299] As mentioned, the angular position of a scattered peak uniquely determines the direction and momentum of the scattering phonon; therefore, localizing the incident beam necessarily increases the range of angles, resulting in a trade-off of between a more localized, higher spatial resolution measurement with greater uncertainty in spectral resolution. This still allows for the accurate mapping of glassy isotropic systems, such as glassy oxides and polymers[300–302] or biological media[299] to determine mechanical properties and locate interfaces, or in the case of Raman microscopy, determine the distribution of strain in a stressed material.[297,303–304]

Extensions of these characterization tools are pump-probe methods. In these techniques, phonons are induced inside of the material, raising the chances for Anti-Stokes scattering. In fact, the very first BLS experiments by Debye and Sears in 1932 utilized vibrationally stimulated scattering in solvents.[305] A similar technique, impulsive stimulated scattering, creates instantaneous optical gratings by the interference of a pump beam to create periodic thermal expansion in the sample, which in turn propagates as a phonon.[306–310] The subsequent phonon can be monitored by the scattering of a probe beam or pulse in both the time and frequency domain to determine material properties and dispersion at that wavelength. Impulsive stimulated scattering and similar pulse techniques utilizing a wave packet rather than a single grating[311] have been utilized to measure structured materials such as phononic crystals[311–313]

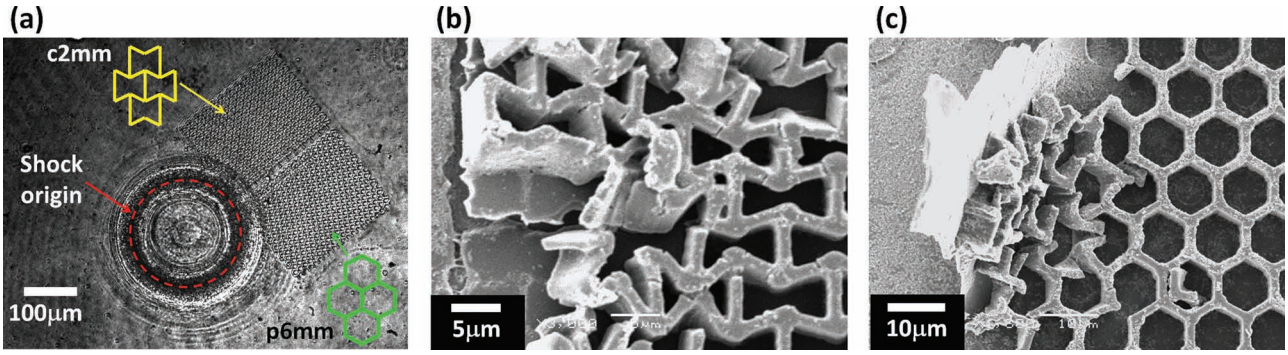

Figure 23. Optical single pulse images of shock tests on MNSMs. Shock excitation indicated by the red dashed lines. (a) Propagating circular shock waves through the MNSMs of different plane groups (c2mm and p6mm). The MNSMs are fabricated by MPL using SU-8 epoxy. SEM images of (b) the c2mm auxetic MNSM and (c) the p6mm MNSM after deformation by the shock waves. The post mortem SEM analysis of indicated area reveals how the structure dissipates the shock by compaction, plasticity and brittle fracture.

and ring resonators.[314] We have more recently investigated a related pump-probe technique for the analysis of the interactions between a MNSM and *non*-linear acoustic waves (i.e. shock waves). In this technique, the probe pulse is tightly focused as a ring or line and propagates in a surrounding liquid towards the sample as a shock wave.[315] The probe pulse (at a non-absorbing wavelength) is appropriately delayed so as to take a nanosecond-exposure-time image of the travelling shock front at a desired time after the initial shock event. We are currently utilizing this technique, which is an intersection between scattering and HSR measurements, to investigate shock on MNSMs fabricated by MPL and IL by both *in situ* and post mortem analysis (**Figure 23**).

5. Summary and Perspectives

In this review we have focused on the mechanical aspects of MNSMs and highlighted new opportunities for MNSM based mechanical metamaterials. Most of the current metamaterials are "handmade" and, therefore, largely at the macroscale. The ability to design and fabricate 2D and 3D metamaterials at the micro- and nano-scale has been greatly increased by recent processing advances, including both large area parallel techniques and high resolution serial techniques and, further, via a rapidly increasing catalog of hybrid techniques possessing the advantages of each. Such structures with sufficiently small lattice constants will enable metamaterials for high frequency applications. Methods for the analysis of properties of mechanical metamaterials have also been improved, with upcoming methods for measuring and modeling even HSR or shock responses of MSNM. Utilizing these advances, diverse devices ranging from variable particle filters to acoustic cloaks have been successfully fabricated; however, relative to other similar research areas, such as optical metamaterials or the mature field of semiconductor electronics, research and applications of mechanical metamaterials are still largely unexplored. Due to the wide range of materials properties, the complex tensorial nature of mechanical responses, and the increasing body of theoretical work, the potential for future development and innovation, utilizing new fabrication tools is immense. It is expected that the nature of mechanical applications will certainly require the scaling up of MNSM production to meet real engineering goals. In spite of many challenges, we optimistically foresee that these issues will be overcome by close collaborations between the science and engineering communities to fully exploit the opportunities arising from the successful manipulation of MNSM-based metamaterials.

Acknowledgements

This research was supported (in part) by the U.S. Army Research Office to the Institute for Soldier Nanotechnologies at MIT under contract W911NF-07-D-0004. Funding from the National Science Foundation (DMR 0804449) and as well as from Asian Office of Air Force Research and Development and the Singapore Defense Science Office are gratefully acknowledged. Helpful technical discussions with Dr. H. Koh, Professor L. Wang, and Professor M. Boyce are also acknowledged.

Received: April 24, 2012
Revised: May 21, 2012
Published online: August 17, 2012

[1] O. D. Sherby, J. Wadsworth, *J. Mater. Process. Technol.* **2001**, *117*, 347.
[2] J. A. Wert, X. X. Huang, G. Winther, W. G. Pantleon, H. F. Poulsen, *Mater. Today* **2007**, *10*, 24.
[3] A. S. Argon, S. Yip, *Philos. Mag. Lett.* **2006**, *86*, 713.
[4] M. M. Schwartz, *Composite materials handbook*, McGraw-Hill, New York **1992**.
[5] *Concise Encyclopedia of Composite Materials* (Ed: A. Mortensen), Elsevier, Amsterdam **2007**.
[6] G. W. Milton, *The Theory of Composites*, Cambridge University Press, Cambridge **2002**.
[7] *Mechanics of Composite Materials and Structures* (Eds: C. A. Mota Soares, C. M. Mota Soares, M. J. M. Freitas), Kluwer Academic Publishers, Dordrecht **1999**.
[8] J. B. Pendry, A. J. Holden, W. J. Stewart, I. Youngs, *Phys. Rev. Lett.* **1996**, *76*, 4773.
[9] J. B. Pendry, A. J. Holden, D. J. Robbins, W. J. Stewart, *IEEE Trans. Microw. Theory Tech.* **1999**, *47*, 2075.
[10] D. R. Smith, W. J. Padilla, D. C. Vier, S. C. Nemat-Nasser, S. Schultz, *Phys. Rev. Lett.* **2000**, *84*, 4184.

[11] K. A. Arpin, A. Mihi, H. T. Johnson, A. J. Baca, J. A. Rogers, J. A. Lewis, P. V. Braun, *Adv. Mater.* **2010**, *22*, 1084.
[12] Silicon ingot (www.3teshop.com/images/Silicon%202.jpg); Photonic crystal (www.sandia.gov/media/images/jpg/lattice.jpg); Microprocessor (www.develop3d.com/uploaded_images/Intel-718028.jpg).
[13] L. J. Gibson, M. F. Ashby, *Cellular solids*, Cambridge University Press, Cambridge **1997**.
[14] M. F. Ashby, A. G. Evans, N. A. Fleck, L. J. Gibson, J. W. Hutchinson, H. N. G. Wadley, *Metal Foams: A Design Guide*, Butterworth-Heinemann, Boston **2000**.
[15] N. C. Gallego, J. W. Klett, *Carbon* **2003**, *41*, 1461.
[16] X. D. Li, W. C. Chang, Y. J. Chao, R. Z. Wang, M. Chang, *Nano Lett.* **2004**, *4*, 613.
[17] D. Raabe, P. Romano, C. Sachs, H. Fabritius, A. Al-Sawalmih, S. Yi, G. Servos, H. G. Hartwig, *Mat. Sci. Eng. A-Struct.* **2006**, *421*, 143.
[18] J. Seto, H. S. Gupta, P. Zaslansky, H. D. Wagner, P. Fratzl, *Adv. Funct. Mater.* **2008**, *18*, 1905.
[19] T. M. Keaveny, E. F. Morgan, G. L. Niebur, O. C. Yeh, *Annu. Rev. Biomed. Eng.* **2001**, *3*, 307.
[20] L. J. Gibson, M. F. Ashby, *Proc. R. Soc. Lond. A* **1982**, *382*, 43.
[21] M. F. Ashby, *Philos. T. R. Soc. A* **2006**, *364*, 15.
[22] M. Maldovan, C. K. Ullal, J. H. Jang, E. L. Thomas, *Adv. Mater.* **2007**, *19*, 3809.
[23] M. Maldovan, C. K. Ullal, W. C. Carter, E. L. Thomas, *Nat. Mater.* **2003**, *2*, 664.
[24] J.-H. Lee, L. F. Wang, S. Kooi, M. C. Boyce, E. L. Thomas, *Nano Lett.* **2010**, *10*, 2592.
[25] L. F. Wang, M. C. Boyce, C. Y. Wen, E. L. Thomas, *Adv. Funct. Mater.* **2009**, *19*, 1343.
[26] H. S. Ma, A. P. Roberts, J. H. Prevost, R. Jullien, G. W. Scherer, *J. Non-Cryst. Solids* **2000**, *277*, 127.
[27] T. A. Schaedler, A. J. Jacobsen, A. Torrents, A. E. Sorensen, J. Lian, J. R. Greer, L. Valdevit, W. B. Carter, *Science* **2011**, *334*, 962.
[28] L. P. Lefebvre, J. Banhart, D. C. Dunand, *Adv. Eng. Mater.* **2008**, *10*, 775.
[29] A. R. Studart, U. T. Gonzenbach, E. Tervoort, L. J. Gauckler, *J. Am. Ceram. Soc.* **2006**, *89*, 1771.
[30] L. Valdevit, A. J. Jacobsen, J. R. Greer, W. B. Carter, *J. Am. Ceram. Soc.* **2011**, *94*, 1.
[31] D. R. Clarke, *J. Am. Ceram. Soc.* **1992**, *75*, 739.
[32] L. F. Wang, J. Lau, E. L. Thomas, M. C. Boyce, *Adv. Mater.* **2011**, *23*, 1524.
[33] K. Tai, M. Dao, S. Suresh, A. Palazoglu, C. Ortiz, *Nat. Mater.* **2007**, *6*, 454.
[34] A. J. Jacobsen, S. Mahoney, W. B. Carter, S. Nutt, *Carbon* **2011**, *49*, 1025.
[35] D. B. Burckel, C. M. Washburn, A. K. Raub, S. R. J. Brueck, D. R. Wheeler, S. M. Brozik, R. Polsky, *Small* **2009**, *5*, 2792.
[36] A. A. Zakhidov, R. H. Baughman, Z. Iqbal, C. X. Cui, I. Khayrullin, S. O. Dantas, I. Marti, V. G. Ralchenko, *Science* **1998**, *282*, 897.
[37] J.-H. Lee, L. F. Wang, M. C. Boyce, E. L. Thomas, **2012**, (submitted).
[38] N. J. Petch, *J. Iron Steel Inst.* **1953**, *174*, 25.
[39] F. Dalla Torre, H. Van Swygenhoven, M. Victoria, *Acta Mater.* **2002**, *50*, 3957.
[40] J. R. Trelewicz, C. A. Schuh, *Acta Mater.* **2007**, *55*, 5948.
[41] M. Maldovan, E. L. Thomas, *Periodic Materials and Interference Lithography*, Wiley-VCH, Weinheim **2009**.
[42] T. Gorishnyy, M. Maldovan, C. Ullal, E. Thomas, *Phys. World* **2005**, *18*, 24.
[43] W. Cheng, J. J. Wang, U. Jonas, G. Fytas, N. Stefanou, *Nat. Mater.* **2006**, *5*, 830.
[44] S. Mohammadi, A. A. Eftekhar, A. Khelif, W. D. Hunt, A. Adibi, *Appl. Phys. Lett.* **2008**, *92*, 221905.
[45] T. Gorishnyy, J. H. Jang, C. Koh, E. L. Thomas, *Appl. Phys. Lett.* **2007**, *91*, 121915.
[46] T. Still, G. Gantzounis, D. Kiefer, G. Hellmann, R. Sainidou, G. Fytas, N. Stefanou, *Phys. Rev. Lett.* **2011**, *106*, 175505.
[47] J. R. Willis, *Proc. R. Soc. A* **2011**, *467*, 1865.
[48] Z. Liu, X. Zhang, Y. Mao, Y. Y. Zhu, Z. Yang, C. T. Chan, P. Sheng, *Science* **2000**, *289*, 1734.
[49] N. Fang, D. Xi, J. Xu, M. Ambati, W. Srituravanich, C. Sun, X. Zhang, *Nat. Mater.* **2006**, *5*, 452.
[50] J. Li, C. T. Chan, *Phys. Rev. E* **2004**, *70*, 055602.
[51] Z. Y. Liu, C. T. Chan, P. Sheng, *Phys. Rev. B* **2005**, *71*, 014103.
[52] Y. Q. Ding, Z. Y. Liu, C. Y. Qiu, J. Shi, *Phys. Rev. Lett.* **2007**, *99*, 093904.
[53] Z. Liang, J. Li, *Phys. Rev. Lett.* **2012**, *108*, 114301.
[54] S. Zhang, L. Yin, N. Fang, *Phys. Rev. Lett.* **2009**, *102*, 194301.
[55] S. Zhang, C. Xia, N. Fang, *Phys. Rev. Lett.* **2011**, *106*, 024301.
[56] D. Schurig, J. J. Mock, B. J. Justice, S. A. Cummer, J. B. Pendry, A. F. Starr, D. R. Smith, *Science* **2006**, *314*, 977.
[57] N. Stenger, M. Wilhelm, M. Wegener, *Phys. Rev. Lett.* **2012**, *108*, 014301.
[58] L. D. Hicks, M. S. Dresselhaus, *Phys. Rev. B* **1993**, *47*, 12727.
[59] W. Kim, J. Zide, A. Gossard, D. Klenov, S. Stemmer, A. Shakouri, A. Majumdar, *Phys. Rev. Lett.* **2006**, *96*, 045901.
[60] M. S. Dresselhaus, G. Chen, M. Y. Tang, R. G. Yang, H. Lee, D. Z. Wang, Z. F. Ren, J. P. Fleurial, P. Gogna, *Adv. Mater.* **2007**, *19*, 1043.
[61] M. Maldovan, *J. Appl. Phys.* **2011**, *110*, 034308.
[62] E. L. Thomas, D. M. Anderson, C. S. Henkee, D. Hoffman, *Nature* **1988**, *334*, 598.
[63] A. M. Urbas, M. Maldovan, P. DeRege, E. L. Thomas, *Adv. Mater.* **2002**, *14*, 1850.
[64] H.-Y. Hsueh, H.-Y. Chen, M.-S. She, C.-K. Chen, R.-M. Ho, S. Gwo, H. Hasegawa, E. L. Thomas, *Nano Lett.* **2010**, *10*, 4994.
[65] S. Vignolini, N. A. Yufa, P. S. Cunha, S. Guldin, I. Rushkin, M. Stefik, K. Hur, U. Wiesner, J. J. Baumberg, U. Steiner, *Adv. Mater.* **2011**, *OP23*.
[66] S. Basu, Z. M. Zhang, C. J. Fu, *Inter. J. Energy Res.* **2009**, *33*, 1203.
[67] J. P. Mulet, K. Joulain, R. Carminati, J. J. Greffet, *Appl. Phys. Lett.* **2001**, *78*, 2931.
[68] L. Hu, A. Narayanaswamy, X. Y. Chen, G. Chen, *Appl. Phys. Lett.* **2008**, *92*, 133106.
[69] C. Dames, *J. Heat Trans.-T. ASME* **2009**, *131*, 061301.
[70] J. G. Fleming, S. Y. Lin, I. El-Kady, R. Biswas, K. M. Ho, *Nature* **2002**, *417*, 52.
[71] S. Y. Lin, J. G. Fleming, I. El-Kady, *Opt. Lett.* **2003**, *28*, 1683.
[72] S. Y. Lin, J. G. Fleming, I. El-Kady, *Appl. Phys. Lett.* **2003**, *83*, 593.
[73] S. Enoch, G. Tayeb, P. Sabouroux, N. Guerin, P. Vincent, *Phys. Rev. Lett.* **2002**, *89*, 213902.
[74] J. C. W. Lee, C. T. Chan, *Appl. Phys. Lett.* **2007**, *90*, 051912.
[75] J.-H. Lee, J. C. W. Lee, W. Leung, M. Li, K. Constant, C. T. Chan, K. M. Ho, *Adv. Mater.* **2008**, *20*, 3244.
[76] J.-H. Lee, W. Leung, T. G. Kim, K. Constant, K. M. Ho, *Opt. Express* **2008**, *16*, 8742.
[77] J.-H. Lee, Y. S. Kim, K. Constant, K. M. Ho, *Adv. Mater.* **2007**, *19*, 791.
[78] P. Nagpal, S. E. Han, A. Stein, D. J. Norris, *Nano Lett.* **2008**, *8*, 3238.
[79] P. Nagpal, D. P. Josephson, N. R. Denny, J. DeWilde, D. J. Norris, A. Stein, *J. Mater. Chem.* **2011**, *21*, 10836.
[80] K. E. Evans, M. A. Nkansah, I. J. Hutchinson, S. C. Rogers, *Nature* **1991**, *353*, 124.
[81] K. E. Evans, A. Alderson, *Adv. Mater.* **2000**, *12*, 617.
[82] A. Bezazi, F. Scarpa, *Int. J. Fatigue* **2007**, *29*, 922.
[83] A. Alderson, J. Rasburn, S. Ameer-Beg, P. G. Mullarkey, W. Perrie, K. E. Evans, *Ind. Eng. Chem. Res.* **2000**, *39*, 654.

[84] J. Rasburn, P. G. Mullarkey, K. E. Evans, A. Alderson, S. Ameer-Beg, W. Perrie, *AICHE J.* **2001**, *47*, 2623.
[85] J. B. Choi, R. S. Lakes, *Cell. Polym.* **1991**, *10*, 205.
[86] G. E. Stavroulakis, *Phys. Status Solidi B* **2005**, *242*, 710.
[87] M. Bianchi, F. Scarpa, C. W. Smith, *Acta Mater.* **2010**, *58*, 858.
[88] B. Howell, P. Prendergast, L. Hansen, *Appl. Acoust.* **1994**, *43*, 141.
[89] F. Scarpa, L. G. Ciffo, J. R. Yates, *Smart Mater. Struct.* **2004**, *13*, 49.
[90] R. H. Baughman, J. M. Shacklette, A. A. Zakhidov, S. Stafstrom, *Nature* **1998**, *392*, 362.
[91] R. H. Baughman, D. S. Galvao, *Nature* **1993**, *365*, 735.
[92] J. N. Grima, J. J. Williams, K. E. Evans, *Chem. Commun.* **2005**, 4065.
[93] N. R. Keskar, J. R. Chelikowsky, *Nature* **1992**, *358*, 222.
[94] R. Lakes, *Science* **1987**, *235*, 1038.
[95] J. B. Choi, R. S. Lakes, *J. Mater. Sci.* **1992**, *27*, 4678.
[96] B. Xu, F. Arias, S. T. Brittain, X. M. Zhao, B. Grzybowski, S. Torquato, G. M. Whitesides, *Adv. Mater.* **1999**, *11*, 1186.
[97] H. Mitschke, J. Schwerdtfeger, F. Schury, M. Stingl, C. Korner, R. F. Singer, V. Robins, K. Mecke, G. E. Schroder-Turk, *Adv. Mater.* **2011**, *23*, 2669.
[98] O. Levy, S. Krylov, I. Goldfarb, *Smart Mater. Struct.* **2006**, *15*, 1459.
[99] M. Bowick, A. Cacciuto, G. Thorleifsson, A. Travesset, *Phys. Rev. Lett.* **2001**, *87*, 148103.
[100] F. Milstein, K. Huang, *Phys. Rev. B* **1979**, *19*, 2030.
[101] Z. A. D. Lethbridge, J. J. Williams, R. I. Walton, C. W. Smith, R. M. Hooper, K. E. Evans, *Acta Mater.* **2006**, *54*, 2533.
[102] N. Gaspar, C. W. Smith, A. Alderson, J. N. Grima, K. E. Evans, *J. Mater. Sci.* **2011**, *46*, 372.
[103] P. V. Pikhitsa, M. Choi, H. J. Kim, S. H. Ahn, *Phys. Status Solidi B* **2009**, *246*, 2098.
[104] T. P. Hughes, A. Marmier, K. E. Evans, *Int. J. Solids Struct.* **2010**, *47*, 1469.
[105] T. Bückmann, N. Stenger, M. Kadic, J. Kaschke, A. Frölich, T. Kennerknecht, C. Eberl, M. Thiel, M. Wegener, *Adv. Mater.* **2012**, DOI: 10.1002/adma.201200584.
[106] L. F. Wang, M. C. Boyce, *Adv. Funct. Mater.* **2010**, *20*, 3025.
[107] W. J. Carter, S. P. Marsh, *Hugoniot equation of state of polymers* LA-13006-MS, **1995**.
[108] D. A. Shockey, D. R. Curran, P. S. Decarli, *J. Appl. Phys.* **1975**, *46*, 3766.
[109] K. J. Hemker, M. W. Chen, J. W. McCauley, *Science* **2003**, *299*, 1563.
[110] H. Ikeda, Y. Qi, T. Cagin, K. Samwer, W. L. Johnson, W. A. Goddard, *Phys. Rev. Lett.* **1999**, *82*, 2900.
[111] D. X. Wang, J. W. Zhao, S. Hu, X. Yin, S. Liang, Y. H. Liu, S. Y. Deng, *Nano Lett.* **2007**, *7*, 1208.
[112] C. Daraio, V. F. Nesterenko, J. F. Aubuchon, S. H. Jin, *Nano Lett.* **2004**, *4*, 1915.
[113] S. R. Bakshi, V. Singh, D. G. McCartney, S. Seal, A. Agarwala, *Scripta Mater.* **2008**, *59*, 499.
[114] Z. W. Huang, H. Z. Li, Z. L. Pan, Q. M. Wei, Y. J. Chao, X. D. Li, *Sci. Rep.* **2011**, *1*, 1.
[115] H. Shelton, C. D. Hendricks, R. F. Wuerker, *J. Appl. Phys.* **1960**, *31*, 1243.
[116] A. Mocker, S. Bugiel, S. Auer, G. Baust, A. Colette, K. Drake, K. Fiege, E. Grun, F. Heckmann, S. Helfert, J. Hillier, S. Kempf, G. Matt, T. Mellert, T. Munsat, K. Otto, F. Postberg, H. P. Roser, A. Shu, Z. Sternovsky, R. Srama, *Rev. Sci. Instrum.* **2011**, *82*, 095111.
[117] S. Watson, M. J. Gifford, J. E. Field, *J. Appl. Phys.* **2000**, *88*, 65.
[118] R. Verker, N. Eliaz, I. Gouzman, S. Eliezer, M. Fraenkel, S. Maman, F. Beckmann, K. Pranzas, E. Grossman, *Acta Mater.* **2004**, *52*, 5539.
[119] N. T. Kattamis, P. E. Purnick, R. Weiss, C. B. Arnold, *Appl. Phys. Lett.* **2007**, *91*, 171120.
[120] P. Serra, M. Colina, J. M. Fernandez-Pradas, L. Sevilla, J. L. Morenza, *Appl. Phys. Lett.* **2004**, *85*, 1639.
[121] V. Tsouti, C. Boutopoulos, D. Goustouridis, I. Zergioti, P. Normand, D. Tsoukalas, S. Chatzandroulis, *Sensor Actuat. B-Chem.* **2010**, *150*, 148.
[122] M. Ruzzene, F. Scarpa, F. Soranna, *Smart Mater. Struct.* **2003**, *12*, 363.
[123] O. Thorp, M. Ruzzene, A. Baz, *Smart Mater. Struct.* **2001**, *10*, 979.
[124] J. F. Robillard, O. B. Matar, J. O. Vasseur, P. A. Deymier, M. Stippinger, A. C. Hladky-Hennion, Y. Pennec, B. Djafari-Rouhani, *Appl. Phys. Lett.* **2009**, *95*, 124104.
[125] A. Sato, Y. Pennec, N. Shingne, T. Thurn-Albrecht, W. Knoll, M. Steinhart, B. Djafari-Rouhani, G. Fytas, *ACS Nano* **2010**, *4*, 3471.
[126] K. L. Jim, C. W. Leung, S. T. Lau, S. H. Choy, H. L. W. Chan, *Appl. Phys. Lett.* **2009**, *94*, 193501.
[127] Y. W. Yao, F. G. Wu, X. Zhang, Z. L. Hou, *J. Appl. Phys.* **2011**, 110.
[128] D. Melekaslan, F. Kasapoglu, K. Ito, Y. Yagci, O. Okay, *Polym. Int.* **2004**, *53*, 237.
[129] Y. Kang, J. J. Walish, T. Gorishnyy, E. L. Thomas, *Nat. Mater.* **2007**, *6*, 957.
[130] W. Cheng, N. Gomopoulos, G. Fytas, T. Gorishnyy, J. Walish, E. L. Thomas, A. Hiltner, E. Baer, *Nano Lett.* **2008**, *8*, 1423.
[131] J.-H. Jang, S. J. Jhaveri, B. Rasin, C. Koh, C. K. Ober, E. L. Thomas, *Nano Lett.* **2008**, *8*, 1456.
[132] J. H. Jang, C. Y. Koh, K. Bertoldi, M. C. Boyce, E. L. Thomas, *Nano Lett.* **2009**, *9*, 2113.
[133] A. Cicek, O. A. Kaya, B. Ulug, *Appl. Acoust.* **2012**, *73*, 28.
[134] C. Xia, H. Lee, N. Fang, *J. Micromech. Microeng.* **2010**, *20*, 085030.
[135] T. Watanabe, M. Akiyama, K. Totani, S. M. Kuebler, F. Stellacci, W. Wenseleers, K. Braun, S. R. Marder, J. W. Perry, *Adv. Funct. Mater.* **2002**, *12*, 611.
[136] L. D. Zarzar, P. Kim, M. Kolle, C. J. Brinker, J. Aizenberg, B. Kaehr, *Angew. Chem. Int. Ed.* **2011**, *50*, 9356.
[137] S. Serak, N. Tabiryan, R. Vergara, T. J. White, R. A. Vaia, T. J. Bunning, *Soft Matter* **2010**, *6*, 779.
[138] K. M. Lee, H. Koerner, R. A. Vaia, T. J. Bunning, T. J. White, *Macromolecules* **2010**, *43*, 8185.
[139] S. V. Serak, N. V. Tabiryan, T. J. White, T. J. Bunning, *Opt. Express* **2009**, *17*, 15736.
[140] Y. Yu, M. Nakano, A. Shishido, T. Shiono, T. Ikeda, *Chem. Mater.* **2004**, *16*, 1637.
[141] T. Ikeda, M. Nakano, Y. Yu, O. Tsutsumi, A. Kanazawa, *Adv. Mater.* **2003**, *15*, 201.
[142] Y. Wu, Y. Lai, Z.-Q. Zhang, *Phys. Rev. Lett.* **2011**, *107*, 105506.
[143] C.-L. Ding, X.-P. Zhao, *J. Phys. D: Appl. Phys.* **2011**, *44*, 215402.
[144] S. Mohammadi, A. A. Eftekhar, A. Khelif, A. Adibi, *Opt. Express* **2010**, *18*, 9164.
[145] S. Mohammadi, A. A. Eftekhar, W. D. Hunt, A. Adibi, *Appl. Phys. Lett.* **2009**, *94*, 051906.
[146] N. Kuo, *Appl. Phys. Lett.* **2011**, *99*, 163501.
[147] X. M. Zhao, Y. N. Xia, G. M. Whitesides, *Adv. Mater.* **1996**, *8*, 837.
[148] S. Y. Lin, J. G. Fleming, D. L. Hetherington, B. K. Smith, R. Biswas, K. M. Ho, M. M. Sigalas, W. Zubrzycki, S. R. Kurtz, J. Bur, *Nature* **1998**, *394*, 251.
[149] M. Qi, E. Lidorikis, P. T. Rakich, S. G. Johnson, J. D. Joannopoulos, E. P. Ippen, H. I. Smith, *Nature* **2004**, *429*, 538.
[150] J.-H. Lee, C. H. Kim, K. M. Ho, K. Constant, *Adv. Mater.* **2005**, *17*, 2481.
[151] K. Aoki, H. T. Miyazaki, H. Hirayama, K. Inoshita, T. Baba, K. Sakoda, N. Shinya, Y. Aoyagi, *Nat. Mater.* **2003**, *2*, 117.
[152] K. Robbie, M. J. Brett, *J. Vac. Sci. Technol. A* **1997**, *15*, 1460.
[153] K. Robbie, M. J. Brett, A. Lakhtakia, *Nature* **1996**, *384*, 616.
[154] D. X. Ye, Z. P. Yang, A. S. P. Chang, J. Bur, S. Y. Lin, T. M. Lu, R. Z. Wang, S. John, *J. Phys. D: Appl. Phys.* **2007**, *40*, 2624.

[155] M. Malac, R. F. Egerton, M. J. Brett, B. Dick, *J. Vac. Sci. Technol. B* **1999**, *17*, 2671.
[156] M. J. Brett, M. M. Hawkeye, *Science* **2008**, *319*, 1192.
[157] S. Takahashi, K. Suzuki, M. Okano, M. Imada, T. Nakamori, Y. Ota, K. Ishizaki, S. Noda, *Nat. Mater.* **2009**, *8*, 721.
[158] A. J. Jacobsen, W. Barvosa-Carter, S. Nutt, *Adv. Mater.* **2007**, *19*, 3892.
[159] C. Cuisin, A. Chelnokov, J. M. Lourtioz, D. Decanini, Y. Chen, *Appl. Phys. Lett.* **2000**, *77*, 770.
[160] C. C. Cheng, A. Scherer, *J. Vac. Sci. Technol. B* **1995**, *13*, 2696.
[161] L. Tang, T. Yoshie, *J. Vac. Sci. Technol. B* **2010**, *28*, 301.
[162] A. J. Jacobsen, W. Barvosa-Carter, S. Nutt, *Acta Mater.* **2008**, *56*, 1209.
[163] M. Campbell, D. N. Sharp, M. T. Harrison, R. G. Denning, A. J. Turberfield, *Nature* **2000**, *404*, 53.
[164] C. K. Ullal, M. Maldovan, E. L. Thomas, G. Chen, Y. J. Han, S. Yang, *Appl. Phys. Lett.* **2004**, *84*, 5434.
[165] J. H. Jang, C. K. Ullal, T. Gorishnyy, V. V. Tsukruk, E. L. Thomas, *Nano Lett.* **2006**, *6*, 740.
[166] S. Yang, M. Megens, J. Aizenberg, P. Wiltzius, P. M. Chaikin, W. B. Russel, *Chem. Mater.* **2002**, *14*, 2831.
[167] Y. C. Chen, J. B. Geddes, Iii, J. T. Lee, P. V. Braun, P. Wiltzius, *Appl. Phys. Lett.* **2007**, *91*, 241103.
[168] S. Jeon, D. J. Shir, Y. S. Nam, R. Nidetz, M. Highland, D. G. Cahill, J. A. Rogers, M. F. Su, I. F. El-Kady, C. G. Christodoulou, G. R. Bogart, *Opt. Express* **2007**, *15*, 6358.
[169] C. H. Chang, L. Tian, W. R. Hesse, H. Gao, H. J. Choi, J. G. Kim, M. Siddiqui, G. Barbastathis, *Nano Lett.* **2011**, 2533.
[170] X. Di, P. C. Kevin, H. Ahmad, L. Yuankun, *CLEO* **2010**, CFF3.
[171] J. H. Jang, D. Dendukuri, T. A. Hatton, Edwin L. Thomas, Patrick S. Doyle, *Angew. Chem. Int. Ed.* **2007**, *46*, 9027.
[172] M. C. George, E. C. Nelson, J. A. Rogers, P. V. Bruan, *Angew. Chem. Int. Ed.* **2009**, *48*, 144.
[173] Y. Lin, D. Rivera, K. P. Chen, *Opt. Express* **2006**, *14*, 887.
[174] E. B. Duoss, M. Twardowski, J. A. Lewis, *Adv. Mater.* **2007**, *19*, 3485.
[175] G. M. Gratson, F. García-Santamaría, V. Lousse, M. Xu, S. Fan, J. A. Lewis, P. V. Braun, *Adv. Mater.* **2006**, *18*, 461.
[176] D. J. Lorang, D. Tanaka, C. M. Spadaccini, K. A. Rose, N. J. Cherepy, J. A. Lewis, *Adv. Mater.* **2011**, *23*, 5055.
[177] B. Y. Ahn, D. J. Lorang, J. A. Lewis, *Nanoscale* **2011**, *3*, 2700.
[178] B. Y. Ahn, D. Shoji, C. J. Hansen, E. Hong, D. C. Dunand, J. A. Lewis, *Adv. Mater.* **2010**, *22*, 2251.
[179] W. Wu, A. DeConinck, J. A. Lewis, *Adv. Mater.* **2011**, *23*, H178.
[180] W. Haske, V. W. Chen, J. M. Hales, W. Dong, S. Barlow, S. R. Marder, J. W. Perry, *Opt. Express* **2007**, *15*, 3426.
[181] C. Sun, N. Fang, D. M. Wu, X. Zhang, *Sensor Actuat. A-Phys.* **2005**, *121*, 113.
[182] S. Maruo, K. Ikuta, *Appl. Phys. Lett.* **2000**, *76*, 2656.
[183] J. Fischer, G. von Freymann, M. Wegener, *Adv. Mater.* **2010**, *22*, 3578.
[184] M. Farsari, G. Filippidis, C. Fotakis, *Opt. Lett.* **2005**, *30*, 3180.
[185] M. Deubel, G. Von Freymann, M. Wegener, S. Pereira, K. Busch, C. M. Soukoulis, *Nat. Mater.* **2004**, *3*, 444.
[186] L. Li, R. R. Gattass, E. Gershgoren, H. Hwang, J. T. Fourkas, *Science* **2009**, *324*, 910.
[187] C. N. LaFratta, J. T. Fourkas, T. Baldacchini, R. A. Farrer, *Angew. Chem. Int. Ed.* **2007**, *46*, 6238.
[188] M. Thiel, J. Fischer, G. von Freymann, M. Wegener, *Appl. Phys. Lett.* **2010**, *97*, 221102.
[189] K. K. Seet, S. Juodkazis, V. Jarutis, H. Misawa, *Appl. Phys. Lett.* **2006**, *89*, 024106.
[190] M. Malinauskas, A. Zukauskas, G. Biekauskaite, R. Gadonas, S. Juodkazis, *Opt. Express* **2010**, *18*, 10209.
[191] T. F. Scott, B. A. Kowalski, A. C. Sullivan, C. N. Bowman, R. R. McLeod, *Science* **2009**, *324*, 913.
[192] J. K. Gansel, M. Thiel, M. S. Rill, M. Decker, K. Bade, V. Saile, G. von Freymann, S. Linden, M. Wegener, *Science* **2009**, *325*, 1513.
[193] M. Kadic, T. Bückmann, N. Stenger, M. Thiel, M. Wegener, *Appl. Phys. Lett.* **2012**, *100*, 191901.
[194] G. W. Milton, A. V. Cherkaev, *J. Eng. Mater. Technol.* **1995**, *117*, 483.
[195] C. Yao-Yu, T. Nobuyuki, T. Takuo, D. Xuan-Ming, K. Satoshi, *Small* **2009**, *5*, 1144.
[196] B.-B. Xu, H. Xia, L.-G. Niu, Y.-L. Zhang, K. Sun, Q.-D. Chen, Y. Xu, Z.-Q. Lv, Z.-H. Li, H. Misawa, H.-B. Sun, *Small* **2010**, *6*, 1762.
[197] T. Baldacchini, A.-C. Pons, J. Pons, C. LaFratta, J. Fourkas, Y. Sun, M. Naughton, *Opt. Express* **2005**, *13*, 1275.
[198] F. Stellacci, C. A. Bauer, T. Meyer-Friedrichsen, W. Wenseleers, V. Alain, S. M. Kuebler, S. J. K. Pond, Y. Zhang, S. R. Marder, J. W. Perry, *Adv. Mater.* **2002**, *14*, 194.
[199] S. Shukla, X. Vidal, E. P. Furlani, M. T. Swihart, K.-T. Kim, Y.-K. Yoon, A. Urbas, P. N. Prasad, *ACS Nano* **2011**, *5*, 1947.
[200] Y.-H. Ye, F. LeBlanc, A. Hache, V.-V. Truong, *Appl. Phys. Lett.* **2001**, *78*, 52.
[201] S. B.Juhl, E. P. Chan, Y. H. Ha, M. Maldovan, J. Brunton, V. Ward, T. Dokland, J. Kalmakoff, B. Farmer, E. L. Thomas, R. A. Vaia, *Adv. Funct. Mater.* **2006**, *16*, 1086.
[202] R. C. Hayward, D. A. Saville, I. A. Aksay, *Nature* **2000**, *404*, 56.
[203] N. Harris, et al., *Nanotechnology* **2007**, *18*, 365301.
[204] G. Jianping, H. Yongxing, Y. Yadong, *Angew. Chem. Int. Ed.* **2007**, *46*, 7428.
[205] S. A. Rinne, F. Garcia-Santamaria, P. V. Braun, *Nat. Photonics* **2008**, *2*, 52.
[206] T. Still, W. Cheng, M. Retsch, U. Jonas, G. Fytas, *J. Phys.: Condens. Matter* **2008**, *20*, 404203.
[207] E. L. Thomas, T. Gorishnyy, M. Maldovan, *Nat. Mater.* **2006**, *5*, 773.
[208] J. Yin, M. Retsch, J.-H. Lee, E. L. Thomas, M. C. Boyce, *Langmuir* **2011**, *27*, 10492.
[209] D. V. Talapin, E. V. Shevchenko, M. I. Bodnarchuk, X. Ye, J. Chen, C. B. Murray, *Nature* **2009**, *461*, 964.
[210] A. Dong, J. Chen, P. M. Vora, J. M. Kikkawa, C. B. Murray, *Nature* **2010**, *466*, 474.
[211] S. Grego, T. W. Jarvis, B. R. Stoner, J. S. Lewis, *Langmuir* **2005**, *21*, 4971.
[212] E. Auyeung, J. I. Cutler, R. J. Macfarlane, M. R. Jones, J. S. Wu, G. Liu, K. Zhang, K. D. Osberg, C. A. Mirkin, *Nat. Nanotechnol.* **2012**, *7*, 24.
[213] R. J. Macfarlane, B. Lee, M. R. Jones, N. Harris, G. C. Schatz, C. A. Mirkin, *Science* **2011**, *334*, 204.
[214] M. R. Jones, R. J. Macfarlane, B. Lee, J. A. Zhang, K. L. Young, A. J. Senesi, C. A. Mirkin, *Nat. Mater.* **2010**, *9*, 913.
[215] C. Park, J. Yoon, E. L. Thomas, *Polymer* **2003**, *44*, 6725.
[216] A. Mavroudis, A. Avgeropoulos, N. Hadjichristidis, E. L. Thomas, D. J. Lohse, *Chem. Mater.* **2003**, *15*, 1976.
[217] F. S. Bates, G. H. Fredrickson, *Annu. Rev. Phys. Chem.* **1990**, *41*, 525.
[218] Y. W. Chiang, R. M. Ho, E. L. Thomas, C. Burger, B. S. Hsiao, *Adv. Funct. Mater.* **2009**, *19*, 448.
[219] W. Zheng, Z.-G. Wang, *Macromolecules* **1995**, *28*, 7215.
[220] F. S. Bates, G. H. Fredrickson, *Phys. Today* **1999**, *52*, 32.
[221] M. Bockstaller, R. Kolb, E. L. Thomas, *Adv. Mater.* **2001**, *13*, 1783.
[222] M. Bockstaller, R. A. Mickiewicz, E. L. Thomas, *Adv. Mater.* **2005**, *17*, 1331.
[223] A. M. Urbas, E. L. Thomas, H. Kriegs, G. Fytas, R. S. Penciu, L. N. Economou, *Phys. Rev. Lett.* **2003**, *90*, 108302.
[224] A. Urbas, R. Sharp, Y. Fink, E. L. Thomas, M. Xenidou, L. J. Fetters, *Adv. Mater.* **2000**, *12*, 812.

[225] J. P. Singer, S. E. Kooi, E. L. Thomas, *Nanoscale* **2011**, *3*, 2730
[226] J. Scrimgeour, D. N. Sharp, C. F. Blanford, O. M. Roche, R. G. Denning, A. J. Turberfield, *Adv. Mater.* **2006**, *18*, 1557.
[227] M. C. George, A. Mohraz, M. Piech, N. S. Bell, J. A. Lewis, P. V. Braun, *Adv. Mater.* **2009**, *21*, 66.
[228] J. P. Singer, J.-H. Lee, S. E. Kooi, E. L. Thomas, *Opt. Express* **2012**, *20*, 11097.
[229] S. A. Pruzinsky, P. V. Braun, *Adv. Funct. Mater.* **2005**, *15*, 1995.
[230] V. Ramanan, E. Nelson, A. Brzezinski, P. V. Braun, P. Wiltzius, *Appl. Phys. Lett.* **2008**, *92*, 173304.
[231] M. Li, K. Douki, K. Goto, X. Li, C. Coenjarts, D. M. Smilgies, C. K. Ober, *Chem. Mater.* **2004**, *16*, 3800.
[232] E. C. Nelson, F. Garcia-Santamaria, P. V. Braun, *Adv. Funct. Mater.* **2008**, *18*, 1983.
[233] C. Y. Cho, J. H. Moon, *Adv. Mater.* **2011**, *23*, 2971.
[234] M. P. Stoykovich, H. Kang, K. C. Daoulas, G. Liu, C.-C. Liu, J. J. de Pablo, M. Müller, P. F. Nealey, *ACS Nano* **2007**, *1*, 168.
[235] E. W. Edwards, M. F. Montague, H. H. Solak, C. J. Hawker, P. F. Nealey, *Adv. Mater.* **2004**, *16*, 1315.
[236] J. G. Son, J.-B. Chang, K. K. Berggren, C. A. Ross, *Nano Lett.* **2011**, *11*, 5079.
[237] C. A. Ross, Y. S. Jung, V. P. Chuang, J. G. Son, K. W. Gotrik, R. A. Mickiewicz, J. K. W. Yang, J. B. Chang, K. K. Berggren, J. Gwyther, I. Manners, *Proc. SPIE* **2010**, *7637*, 76370H.
[238] Y. S. Jung, W. Jung, C. A. Ross, *Nano Lett.* **2008**, *8*, 2975.
[239] C. Osuji, P. J. Ferreira, G. P. Mao, C. K. Ober, J. B. Vander Sande, E. L. Thomas, *Macromolecules* **2004**, *37*, 9903.
[240] T. Xu, Y. Q. Zhu, S. P. Gido, T. P. Russell, *Macromolecules* **2004**, *37*, 2625.
[241] D. E. Angelescu, J. H. Waller, D. H. Adamson, P. Deshpande, S. Y. Chou, R. A. Register, P. M. Chaikin, *Adv. Mater.* **2004**, *16*, 1736.
[242] B. C. Berry, A. W. Bosse, J. F. Douglas, R. L. Jones, A. Karim, *Nano Lett.* **2007**, *7*, 2789.
[243] T. Hashimoto, J. Bodycomb, Y. Funaki, K. Kimishima, *Macromolecules* **1999**, *32*, 952.
[244] D. E. Angelescu, J. H. Waller, D. H. Adamson, R. A. Register, P. M. Chaikin, *Adv. Mater.* **2007**, *19*, 2687.
[245] C. De Rosa, C. Park, E. L. Thomas, B. Lotz, *Nature* **2000**, *405*, 433.
[246] C. Park, C. De Rosa, E. L. Thomas, *Macromolecules* **2001**, *34*, 2602.
[247] J. Ye, R. Zentel, S. Arpiainen, J. Ahopelto, F. Jonsson, S. G. Romanov, C. M. Sotomayor Torres, *Langmuir* **2006**, *22*, 7378.
[248] H.-J. Hung, P.-C. Yang, J.-H. Liu, *J. Appl. Polym. Sci.* **2008**, *109*, 3776.
[249] B. H. Jones, T. P. Lodge, *ACS Nano* **2011**.
[250] A. C. Arsenault, D. A. Rider, N. Tetreault, J. I. L. Chen, N. Coombs, G. A. Ozin, I. Manners, *J. Am. Chem. Soc.* **2005**, *127*, 9954.
[251] X. Xiao, T. E. Beechem, M. T. Brumbach, T. N. Lambert, D. J. Davis, J. R. Michael, C. M. Washburn, J. Wang, S. M. Brozik, D. R. Wheeler, D. B. Burckel, R. Polsky, *ACS Nano* **2012**.
[252] P. Jiang, J. F. Bertone, V. L. Colvin, *Science* **2001**, *291*, 453.
[253] R. C. Schroden, M. Al-Daous, C. F. Blanford, A. Stein, *Chem. Mater.* **2002**, *14*, 3305.
[254] Y. Xu, X. Zhu, Y. Dan, J. H. Moon, V. W. Chen, A. T. Johnson, J. W. Perry, S. Yang, *Chem. Mater.* **2008**, *20*, 1816.
[255] N. Tétreault, H. Míguez, G. A. Ozin, *Adv. Mater.* **2004**, *16*, 1471.
[256] F. García-Santamaría, M. Xu, V. Lousse, S. Fan, P. V. Braun, J. A. Lewis, *Adv. Mater.* **2007**, *19*, 1567.
[257] P. V. Braun, P. Wiltzius, *Nature* **1999**, *402*, 603.
[258] J.-H. Lee, C.-H. Kim, Y.-S. Kim, K.-M. Ho, K. Constant, C. H. Oh, *Appl. Phys. Lett.* **2006**, *88*, 181112.
[259] J. B. Pawley, *Handbook of Biological Confocal Microscopy*, Springer Science, New York **2006**.
[260] A. Mohraz, M. J. Solomon, *Langmuir* **2005**, *21*, 5298.
[261] J. Scrimgeour, D. N. Sharp, C. F. Blanford, O. M. Roche, R. G. Denning, A. J. Turberfield, *Adv. Mater.* **2006**, *18*, 1557.
[262] A. Sakellariou, T. J. Sawkins, T. J. Senden, A. Limaye, *Physica A* **2004**, *339*, 152.
[263] Y.-C. Chen, J. B. Geddes III, L. Yin, P. Wiltzius, P. V. Braun, *Adv. Mater.* **2012**, DOI: 10.1002/adma.201200411.
[264] C. G. Schroer, P. Cloetens, M. Rivers, A. Snigirev, A. Takeuchi, W. B. Yun, *MRS Bull.* **2004**, *29*, 157.
[265] J. Y. Buffiere, P. Cloetens, W. Ludwig, E. Maire, L. Salvo, *MRS Bull.* **2008**, *33*, 611.
[266] H. Toda, K. Uesugi, A. Takeuchi, K. Minami, M. Kobayashi, T. Kobayashi, *Appl. Phys. Lett.* **2006**, *89*, 143112.
[267] F. Lasagni, A. Lasagni, M. Engstler, H. P. Degischer, F. Mucklich, *Adv. Eng. Mater.* **2008**, *10*, 62.
[268] S. D. Oosterhout, M. M. Wienk, S. S. van Bavel, R. Thiedmann, L. J. A. Koster, J. Gilot, J. Loos, V. Schmidt, R. A. J. Janssen, *Nat. Mater.* **2009**, *8*, 818.
[269] U. Ziese, K. P. de Jong, A. J. Koster, *Appl. Catal. A* **2004**, *260*, 71.
[270] J. Dupont, G. J. Liu, K. Niihara, R. Kimoto, H. Jinnai, *Angew. Chem. Int. Ed.* **2009**, *48*, 6144.
[271] H. S. Kim, S. O. Hwang, Y. Myung, J. Park, S. Y. Bae, J. P. Ahn, *Nano Lett.* **2008**, *8*, 551.
[272] M. D. Uchic, L. Holzer, B. J. Inkson, E. L. Principe, P. Munroe, *MRS Bull.* **2007**, *32*, 408.
[273] F. Lasagni, A. Lasagni, E. Marks, C. Holzapfel, F. Mucklich, H. P. Degischer, *Acta Mater.* **2007**, *55*, 3875.
[274] Z. Yu, S. Boseck, *Rev. Mod. Phys.* **1995**, *67*, 863.
[275] G. Li, M. John, *Compos.Sci.Technol.* **2008**, *68*, 3337.
[276] T. V. Torchynska, A. V. Hernandez, A. D. Cano, S. Jimenez-Sandoval, S. Ostapenko, M. Mynbaeva, *J. Appl. Phys.* **2005**, *97*, 033507.
[277] F. Lisy, A. Hiltner, E. Baer, J. L. Katz, A. Meunier, *J. Appl. Polym. Sci.* **1994**, *52*, 329.
[278] W.-S. Kwon, M.-J. Yim, K.-W. Paik, S.-J. Ham, S.-B. Lee, *J.Electron. Packaging* **2005**, *127*, 86.
[279] K. Qin, L. Wang, J. Zhang, J. Min, J. Huang, X. Liang, K. Tang, Y. Xia, *Vacuum* **2012**, *86*, 827.
[280] A. C. Fisher-Cripps, *Nanoindentation*, Springer, New York **2004**.
[281] S. Timoshenko, J. N. Goodier, *Theory of Elasticity*, McGraw-Hill, New York **1951**.
[282] S. Juodkazis, V. Mizeikis, K. K. Seet, H. Misawa, U. G. K. Wegst, *Appl. Phys. Lett.* **2007**, *91*, 241904.
[283] W. Cheng, R. Sainidou, P. Burgardt, N. Stefanou, A. Kiyanova, M. Efremov, G. Fytas, P. F. Nealey, *Macromolecules* **2007**, *40*, 7283.
[284] N. Gomopoulos, W. Cheng, M. Efremov, P. F. Nealey, G. Fytas, *Macromolecules* **2009**, *42*, 7164.
[285] R. D. Hartschuh, S. P. Wargacki, H. Xiong, J. Neiswinger, A. Kisliuk, S. Sihn, V. Ward, R. A. Vaia, A. P. Sokolov, *Phys. Rve. E* **2008**, 78.
[286] M. B. Hakim, S. M. Lindsay, J. Powell, *Biopolymers* **1984**, *23*, 1185.
[287] R. S. Penciu, H. Kriegs, G. Petekidis, G. Fytas, E. N. Economou, *J. Chem. Phys.* **2003**, *118*, 5224.
[288] G. Tommaseo, R. S. Penciu, G. Fytas, E. N. Economou, T. Hashimoto, N. Hadjichristidis, *Macromolecules* **2004**, *37*, 5006.
[289] T. Gorishnyy, C. K. Ullal, M. Maldovan, G. Fytas, E. L. Thomas, *Phys. Rev. Lett.* **2005**, 94.
[290] R. J. Nemanich, S. A. Solin, *Phys. Rev. B* **1979**, *20*, 392.
[291] R. J. Nemanich, J. T. Glass, G. Lucovsky, R. E. Shroder, *J. Vac. Sci. Technol. A* **1988**, *6*, 1783.
[292] A. Soukiassian, W. Tian, D. A. Tenne, X. X. Xi, D. G. Schlom, N. D. Lanzillotti-Kimura, A. Bruchhausen, A. Fainstein, H. P. Sun, X. Q. Pan, A. Cros, A. Cantarero, *Appl. Phys. Lett.* **2007**, *90*, 042909.
[293] A. Fainstein, B. Jusserand, V. Thierrymieg, *Phys. Rev. Lett.* **1995**, *75*, 3764.
[294] E. Duval, A. Boukenter, B. Champagnon, *Phys. Rev. Lett.* **1986**, *56*, 2052.

[295] A. M. Rao, E. Richter, S. Bandow, B. Chase, P. C. Eklund, K. A. Williams, S. Fang, K. R. Subbaswamy, M. Menon, A. Thess, R. E. Smalley, G. Dresselhaus, M. S. Dresselhaus, *Science* **1997**, *275*, 187.
[296] A. Zumbusch, G. R. Holtom, X. S. Xie, *Phys. Rev. Lett.* **1999**, *82*, 4142.
[297] P. Puech, F. Demangeot, J. Frandon, C. Pinquier, M. Kuball, V. Domnich, Y. Gogotsi, *J. Appl. Phys.* **2004**, *96*, 2853.
[298] A. Hartschuh, E. J. Sánchez, X. S. Xie, L. Novotny, *Phys. Rev. Lett.* **2003**, *90*, 095503.
[299] G. Scarcelli, S. H. Yun, *Nat. Photonics* **2008**, *2*, 39.
[300] J. K. Krüger, W. Possart, R. Bactavachalou, U. Müller, T. Britz, R. Sanctuary, P. Alnot, *J. Adhesion* **2004**, *80*, 585.
[301] R. Sanctuary, B. Ravi, M. Ulrich, W. Possart, P. Alnot, J. K. Krüger, *J. Phys. D: Appl. Phys.* **2003**, *36*, 2738.
[302] Y. Takagi, K. Kurihara, *Rev. Sci. Instrum.* **1992**, *63*, 5552.
[303] J. Menendez, P. Gopalan, G. S. Spencer, N. Cave, J. W. Strane, *Appl. Phys. Lett.* **1995**, *66*, 1160.
[304] Y. N. Wang, C. Galiotis, D. L. Bader, *J. Biomech.* **2000**, *33*, 483.
[305] P. Debye, F. W. Sears, *Proc. Natl. Acad. Sci. USA* **1932**, *18*, 409.
[306] J. A. Rogers, A. Maznev, K. A. Nelson, in *Characterization of Materials*, John Wiley & Sons, Inc., **2002**.
[307] A. A. Maznev, A. Akthakul, K. A. Nelson, *J. Appl. Phys.* **1999**, *86*, 2818.
[308] J. A. Rogers, K. A. Nelson, *J. Appl. Phys.* **1994**, *75*, 1534.
[309] H. Furuta, Y. Tsujimi, Y. Shimada, T. Yagi, *J. Phys. Soc. Jpn. 64*, 4113.
[310] L.-T. Cheng, K. A. Nelson, *Phys. Rev. B* **1988**, *37*, 3603.
[311] Y. Sugawara, O. B. Wright, O. Matsuda, *Rev. Sci. Instrum.* **2003**, *74*, 519.
[312] L. Dhar, J. A. Rogers, *Appl. Phys. Lett.* **2000**, *77*, 1402.
[313] G. Saini, T. Pezeril, J. Torchinsky, J. Yoon, S. Kooi, E. L. Thomas, K. A. Nelson, *J. Mater. Res.* **2007**, *22*, 719.
[314] A. A. Maznev, *Ultrasonics* **2009**, *49*, 1.
[315] T. Pezeril, G. Saini, D. Veysset, S. Kooi, P. Fidkowski, R. Radovitzky, K. A. Nelson, *Phys. Rev. Lett.* **2011**, *106*, 214503.